

# Stable Synchronous Propagation in Feedforward Networks for Biped Locomotion

Ian Stewart and David Wood  
 Mathematics Institute  
 University of Warwick  
 Coventry CV4 7AL  
 United Kingdom

June 16, 2025

## Abstract

Rhythmic gait patterns in animal locomotion are widely believed to be produced by a central pattern generator (CPG), a network of neurons that drives the muscle groups. In previous papers we have discussed how phase-synchronous signals can propagate along chains of neurons using a feedforward lift of the CPG, given sufficient conditions for stability to synchrony-breaking perturbations, and shown that stable signals are common for four standard neuron models. Here we apply these ideas to biped locomotion using a fifth model: Wilson–Cowan (or rate model) neurons. Feedforward architecture propagates the phase pattern of a CPG along a chain of identical modules. For certain rate models, we give analytic conditions that are sufficient for transverse Liapunov and Floquet stability. We compare different notions of transverse stability, summarise some numerical simulations, and outline an application to signal propagation in a model of biped locomotion.

## 1 Introduction

The observation that legged animals move using a variety of rhythmic patterns goes back at least to Aristotle [3], who wondered whether a trotting horse can be completely off the ground during some stages of its motion. His answer (‘no’) was disproved by Muybridge [79], who invented a camera with a rapid shutter and used lines of such cameras, triggered by tripwires, to photograph animals and humans in motion. It is often claimed that this allowed Leland Stanford Jr. to win a large wager (a figure of \$25,000 to \$50,000 is typical), but Stanford was not a betting man and no money was involved [18]. However, the same source cites evidence that he was in a dispute with Frederick McCrellish about this question.

Such patterns of movement are called *gaits* [39, 26]. They also occur for organisms such as arthropods (especially centipedes and millipedes), snakes, worms, and lampreys.

It is widely accepted that the underlying rhythms of gaits arise from the dynamics of a *central pattern generator* (CPG), a neural ‘circuit’ that naturally produces oscillatory patterns. A recent survey is [6], and the prevailing paradigm of alternating activity in excitatory and inhibitory neurons is laid out in [2, 74]. Observations challenging some aspects of this paradigm are described in [66]; they do not affect this paper.

CPG networks have been observed in some organisms, and inferred in many others. In vertebrates the CPG appears to reside in the spinal cord. The CPG rhythms drive the muscle groups that cause motion. Many gaits are ‘symmetric’ [69]: the movements of distinct legs are synchronised, or are related by phase shifts that are a simple fraction of the overall period. An example, the quadruped walk gait, is shown in Figure 1. The legs move in the sequence left rear, left front, right rear, right front, separated by one quarter of the period of the overall gait cycle.

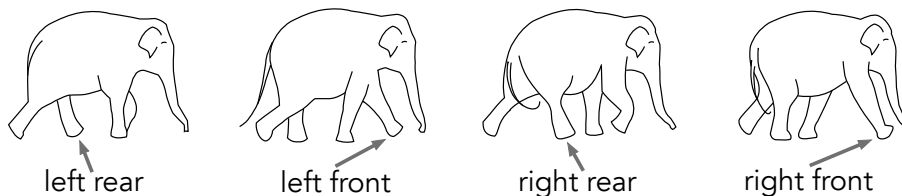


Figure 1: Walk of an elephant: successive legs hit the ground at  $\frac{1}{4}$ -period intervals.

## 1.1 Biped Gaits

In this paper we examine a simpler case, that of bipeds. The most obvious CPG model for  $n$ -legged animals is a network with  $n$  nodes, whose topology is constructed to create the phase patterns typically observed in gaits [16, 17]. However, such a model for quadrupeds ( $n = 4$ ) predicts that the trot and pace gaits are ‘dynamically conjugate’—related by an element of the symmetry group of the model ODE—so they should coexist for all parameter values. This is inconsistent with observations—for example, some breeds of horse, especially those bred for harness racing, can trot but not pace [45]. A proposed modification [34, 35], derived from known features of quadruped gaits, doubles the number of nodes to  $2n$ . Each leg corresponds to two nodes of the network, interpreted as controlling two muscle groups: flexors and extensors. The resulting CPG architecture has  $\mathbb{Z}_n \times \mathbb{Z}_2$  symmetry: an  $n$ -cycle on each side of the animal combined with left-right symmetry. This  $n$ -cycle controls the  $n/2$  legs on the corresponding side of the animal, so there are two nodes per leg. This topology leads to several predictions that are consistent with observations, including half-integer wave numbers in arthropod gaits.

Pinto and Golubitsky [87] analysed the corresponding network model of a CPG for bipeds ( $n = 2$ ): a 4-node CPG with  $\mathbb{Z}_2 \times \mathbb{Z}_2$  symmetry, Figure 2. We have rotated their figure through a right angle and relabelled the nodes, for consistency with later networks. In their model, two nodes control extensor and flexor muscle groups of the ankle of the left leg, and the other two control extensor and flexor muscle groups of the ankle of the right leg. The activity of these muscles and the corresponding ankle movements are idealised, so that the muscles either act in synchrony or are separated by a half-period

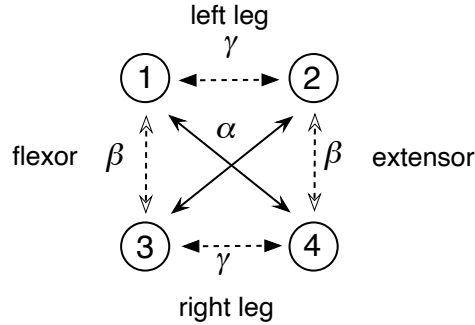


Figure 2: A 4-node CPG network for bipedal gaits, proposed in [87].

phase shift. This idealisation is reasonably close to reality, see [71, 72]. Other muscle groups of course play a role, but are not represented in the model.

The  $H/K$  Theorem of [9] (originally motivated by gait patterns and generalised to arbitrary symmetric dynamical systems) classifies the possible phase patterns in a dynamical system with symmetry group  $\Gamma$  in terms of pairs of subgroups  $H \subseteq K$  of  $\Gamma$ . Here  $K$  is the group of pointwise symmetries of the periodic orbit and  $K$  is the group of setwise symmetries. The main condition is that  $K$  must be a normal subgroup of  $H$  with a cyclic group quotient. Other technical conditions are also required.

For the network of Figure 2 the symmetry group is  $\Gamma = \mathbb{Z}_2 \times \mathbb{Z}_2$ , described in Section 1.3. The  $H/K$  Theorem leads to a list of 11 pairs  $(H, K)$ , corresponding to a total of 11 gaits. Of these, four are ‘primary’ gaits, which can occur by generic Hopf bifurcation from the trivial steady state with all legs stationary. These gaits are the (two-legged) *hop*, *walk*, (two-legged) *jump*, and *run*, see Table 1. Again, Section 1.3 provides further details. In primary gaits, all nodes have the same waveform, but with regular phase differences. (This remark applies to the model; in reality the waveforms are only approximately the same.) The remaining seven ‘secondary’ gaits involve either two or four different waveforms. Six of them can be viewed as ‘mode interactions’ between two primary gaits.

gait	(1) left flexor	(2) left extensor	(3) right flexor	(4) right extensor
hop	$x(t)$	$x(t)$	$x(t)$	$x(t)$
walk	$x(t)$	$x(t + \frac{1}{2})$	$x(t + \frac{1}{2})$	$x(t)$
jump	$x(t)$	$x(t + \frac{1}{2})$	$x(t)$	$x(t + \frac{1}{2})$
run	$x(t)$	$x(t)$	$x(t + \frac{1}{2})$	$x(t + \frac{1}{2})$

Table 1: Classification of primary gaits for bipedal locomotion, assuming a CPG as in Figure 2.

A rate model for this CPG is analysed in [94], and the results are summarised in Section 4.1.

The main objective of this paper is to use the methods of [99, 100] to investigate alternative networks that generate the same patterns as the 4-node CPG in Figure 1, but

propagate them along arbitrarily long chains. One of these networks is a ‘feedforward lift’ of the 4-node CPG, Figure 3 (top). The other is *almost* a feedforward lift, except for lateral connections, as in Figure 3 (bottom). The top network is slightly more tractable mathematically. The bottom one is biologically more plausible and we analyse it using similar methods.

The key feature that we analyse is the *stability* of these patterns; not just to synchrony-preserving perturbations, but also to synchrony-breaking perturbations. We consider both Floquet and Liapunov stability, as well as transverse stability of the synchrony subspace; see Section 2.1 for a summary of these notions.

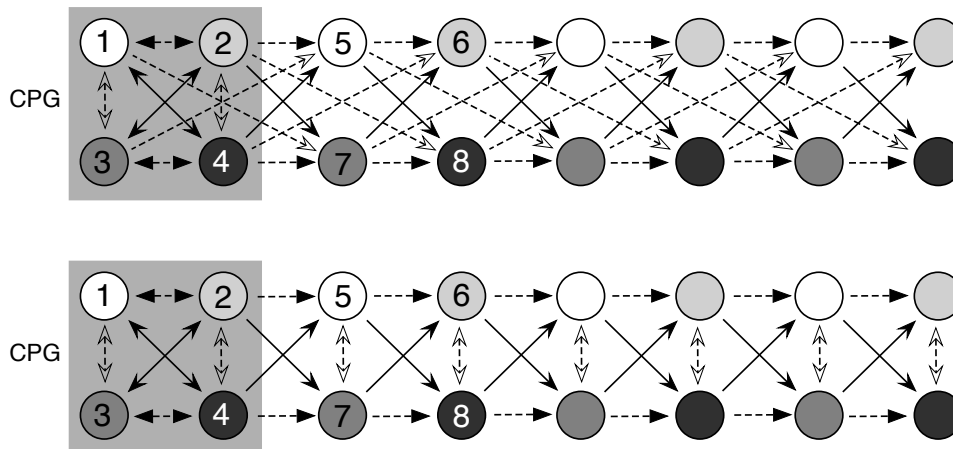


Figure 3: Two lifts of Figure 2, which therefore support the same rhythms. In each subfigure, the top row of nodes corresponds to the left side of the animal and the bottom row to the right side. *Top*: Feedforward lift. *Bottom*: Lift in which all connections to the chain are feedforward except for the lateral ones (vertical double-headed arrows).

## 1.2 Synchrony and Phase Patterns

Regular phase patterns are common in networks of dynamical systems with suitable symmetries [32, 33, 36]. This suggests modelling gait patterns using network dynamics [16, 17]. In network dynamics, each network (labelled directed graph) has an associated set of *admissible* ODEs — ordinary differential equations that are compatible with the network structure in a precise technical sense. In this paper we state explicitly the admissible ODEs for the networks under discussion, so we do not repeat the general definition of ‘admissible’. Full details are in [33, 37, 96]. There is a short summary in [99] and a briefer one in [100].

For modelling purposes, we follow a common convention in the literature and adopt a strong definition of synchrony. Two nodes are *synchronous*, for some admissible ODE, if their waveforms (time series) are identical; they are *phase-synchronous* if their waveforms are identical except for a phase shift (time translation). These definitions are idealisations, but they open up a powerful mathematical approach with useful implications. Real systems can be considered as perturbations of idealised ones, and much of the interesting structure persists in an appropriately approximate form [100, Section 8].

A *synchrony pattern* partitions the nodes of the network into sets that are synchronous, often called *clusters*. A *phase pattern* partitions the nodes of the network into sets that are phase-synchronous, and also assigns specific phase shifts as fractions of the overall period. These patterns are *rigid* if they persist after all sufficiently small admissible perturbations of the ODE. In the phase-synchronous case the period changes under perturbation, so we require the phase shifts to be preserved when measured as fractions of the period. In the context of symmetric dynamics, these ‘spatiotemporal’ symmetries are encoded in two subgroups  $H$  and  $K$  of the symmetry group  $\Gamma$ , where  $K$  is a normal subgroup of  $H$  and  $H/K$  is a finite cyclic group [8, 32]. The group  $K$  determines which nodes are synchronous with each other; the group  $H$  determines the phase shifts when considered modulo  $K$ . In a network version,  $K$  becomes a so-called balanced colouring and  $H$  is a group of symmetries of the corresponding quotient network [33].

The groups  $H$  and  $K$  for Table 1 are listed in [87] and are easily inferred from the table shown. In all cases  $H = \mathbb{Z}_2 \oplus \mathbb{Z}_2$  and  $K$  is equal to  $H$  for the hop and otherwise is one of the three subgroups that are cyclic of order 2. See Example 1.2.

**Example 1.1.** The walk gait of Figure 1 affords a simple example of a phase pattern. Denote the legs by  $LR, LF, RR, RF$  (left rear, left front, right rear, right front). Legs move in that sequence, with successive  $\frac{1}{4}$ -period phase shifts. The synchrony pattern  $K$  is trivial: distinct legs do not synchronise. The symmetry group  $H$  is cyclic of order 4, permuting the legs in the cycle  $(LR, LF, RR, RF)$ . A generator of  $H$  (move one place along the cycle) corresponds to a phase shift  $T/4$  where  $T$  is the overall period.

The bound, pace, and trot gaits (observed in other quadrupeds, [8, 9, 16, 26, 34, 35]) also have nontrivial synchrony/phase patterns. In the bound, the back legs move together and then the front legs move together, so the synchrony clusters  $K$  are  $\{LR, RR\}$  and  $\{LF, RF\}$ . The symmetry group of the clusters is cyclic of order 2, and the phase difference between the clusters is half the period.

The pace and trot are similar, but the synchrony clusters  $K$  are  $\{LR, LF\}$  and  $\{RR, RF\}$  for the pace and  $\{LR, RF\}$  and  $\{RR, LF\}$  for the trot. Again the symmetry group of the clusters is cyclic of order 2, and the phase difference between the clusters is half the period.

### 1.3 Symmetries and CPGs

Phase patterns arise naturally in symmetric dynamical systems [36], leading to the suggestion that gait CPGs should also have appropriate symmetries [17].

**Example 1.2.** Pinto and Golubitsky [87, 94] propose the 4-node network of Figure 2 as a schematic CPG for biped locomotion. A similar model, potentially with less symmetry but the same topology, appears in [1]. The nodes represent neurons or, more realistically, populations of neurons [105]. Although a biped has two legs, the CPG has four nodes. The muscle groups in each leg are activated by two nodes: one flexor and one extensor.

This network has a symmetry group of order 4, comprising the permutations

$$\begin{aligned} \text{id} &= \begin{pmatrix} 1 & 2 & 3 & 4 \\ 1 & 2 & 3 & 4 \end{pmatrix} & \rho &= \begin{pmatrix} 1 & 2 & 3 & 4 \\ 2 & 1 & 4 & 3 \end{pmatrix} \\ \sigma &= \begin{pmatrix} 1 & 2 & 3 & 4 \\ 3 & 4 & 1 & 2 \end{pmatrix} & \rho\sigma &= \begin{pmatrix} 1 & 2 & 3 & 4 \\ 4 & 3 & 2 & 1 \end{pmatrix} \end{aligned}$$

That is: the identity, swap left/right, swap flexor/extensor, swap diagonally. These four permutations constitute the group  $\mathbb{Z}_2 \times \mathbb{Z}_2$ , which corresponds naturally to the observed phase patterns.

CPG architectures of this kind have been explored for bipeds [87, 94], quadrupeds [8, 17, 34, 35, 87, 91], hexapods [16], and arthropods [35], among others. The main techniques are taken from symmetric dynamics: the symmetric Hopf bifurcation theorem [36] and the  $H/K$  theorem [8]. The CPGs that occur in these papers generally have small numbers of neurons (or populations thereof). Typically there are two neurons per leg, for mathematical reasons explained in [34, 35]. A possible biological interpretation is that one neuron (population) is required for extension and one for flexure of the corresponding muscle group.

## 1.4 Classification of Phase Patterns

The assumption of a symmetric CPG is natural in the context of dynamics with symmetry. It is well known that symmetric dynamical systems can generate rigid phase patterns, meaning that the phase shifts concerned remain unchanged (as fractions of the period) after a small symmetry-preserving perturbation [36]. Rigidity is important in biological applications, where precise model equations are seldom available, so meaningful predictions should not depend on fine details of the model. However, there are significant differences between a general symmetric dynamical system and an admissible ODE for a symmetric network [33, Chapter 16]. In particular, the network case permits a more general mechanism to generate rigid phase patterns, without assuming that the network itself is symmetric. Instead, the symmetry occurs in a *quotient network* in which synchronous or phase synchronous nodes are identified. We give a simple example in Section 1.7; this network has only trivial symmetry but it has Figure 2 as a quotient, which has  $\mathbb{Z}_2 \times \mathbb{Z}_2$  symmetry. Thus these network architectures need not correspond directly to physiological ‘wiring diagrams’ (connectomes) in the animal, but could in principle be deduced from wiring diagrams [70].

The rigid phase patterns that can occur in an admissible ODE for a network  $\mathcal{G}$  are characterised by the Network  $H/K$  Theorem [33, Theorem 17.19]. This theorem is a consequence of several highly plausible Rigidity Conjectures [33]. These conjectures have been proved for a wide variety of networks, including all homogeneous and fully inhomogeneous networks [30, 31]. However, those papers makes a tacit assumption that is not always valid [33], so the proof does not apply in full generality. The Rigidity Conjectures have been proved for all networks under additional mild technical conditions [95].

Here  $K$  is a balanced colouring of  $\mathcal{G}$ , determining a rigid synchrony pattern, and  $H$  is a cyclic group  $\mathbb{Z}_r$  of symmetries of the quotient network  $\mathcal{G}^K$  in which synchronous nodes are identified. This kind of symmetry induces phase patterns in which a generator of  $\mathbb{Z}_r$  corresponds to a phase shift of  $mT/r$  where  $T$  is the period and  $m$  is an integer between 0 and  $r - 1$ . The network  $H/K$  Theorem can be viewed as a catalogue of the possible phase patterns; any specific admissible ODE ‘selects’ patterns from this catalogue.

## 1.5 Feedforward Lifts

If a network  $\mathcal{Q}$  is a quotient of a network  $\mathcal{G}$ , we say that  $\mathcal{G}$  is a *lift* of  $\mathcal{Q}$ . Reversing the relation in this manner lets us start from a network  $\mathcal{Q}$  with certain dynamics, such as phase patterns, and construct various lifts  $\mathcal{G}$  in which the corresponding clusters have the same dynamic behaviour as the nodes of  $\mathcal{Q}$ . The Network  $H/K$  Theorem describes a general mathematical scenario in which a phase pattern generated by a simple symmetric network can be lifted to a more complex asymmetric network. The main aim of this paper is to investigate this possibility in the context of the biped CPG of Figure 2, seeking lifts that are biologically more plausible. We focus on a crucial issue: the stability of the lifted state. The basic construction used here is a *feedforward lift*, see Section 2. This construction is discussed in [99] from a general mathematical viewpoint, and [100] analyses a series of ‘toy’ examples based on standard model neurons, again focusing on stability.

The structure of a feedforward lift is motivated by animal physiology. In many animals, oscillations propagate along a chain of neurons, which oscillate in synchrony or phase-synchrony. This architecture generates propagating time-periodic patterns. Synchrony corresponds to a standing wave; phase synchrony to a travelling wave. Legged locomotion in animals is the key example for this paper. Other examples are locomotion in *Drosophila* larvae [29] and the nematode *Caenorhabditis elegans* [82, 90], peristaltic waves in the intestine [13, 14, 25, 40, 59], and the heartbeat of the leech [12, 11, 102, 103].

Such patterns are found elsewhere: for instance to propel continuum robots for medicine [52, 92, 106] or exploration [77]. Gene regulatory networks (GRNs) also exhibit synchrony patterns, and chains of regulatory links can act as delay lines (Leifer *et al.* [64]) leading to phase patterns. The states of GRNs are usually equilibria, but periodic oscillations are also found [88]. Elowitz and Leibler [20] found phase-synchronous patterns in the repressilator, a synthetic genetic circuit. In an idealised model these patterns are a consequence of  $\mathbb{Z}_3$  symmetry [70, 98].

## 1.6 Example: the Leech Heartbeat

Figure 4 shows a neural circuit for the heartbeat of the medicinal leech *Hirudo medicinalis* based on observations in Kristan *et al.* [58]. A CPG (shaded) with 14 interneurons (HN) generates rhythmic signals that propagate along two chains of heart excitatory neurons (HE). This network is a feedforward lift of the CPG, except for the HE nodes 3–7, which have slightly different inputs from HE nodes 8 onwards.

A curious feature of the leech’s heartbeat is that contractions occur as a standing wave along one side of the animal, but as a travelling wave along the other. After about

20–40 heartbeat cycles the two patterns swap sides [11, 58]. We do not investigate this kind of switching here; see [10, 83] for two possible explanations.

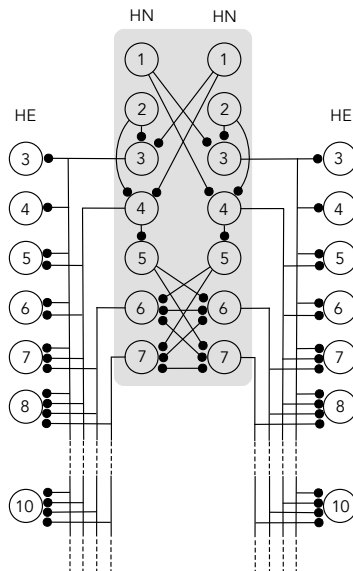


Figure 4: Neural circuit for the heartbeat of the medicinal leech, after [58]. Nodes in the shaded box form the CPG. HN = heart interneuron, HE = heart excitatory neuron.

## 1.7 Asymmetric CPGs can Generate Phase Patterns

The feedforward lifts in Figure 3 preserve the  $\mathbb{Z}_2 \times \mathbb{Z}_2$  symmetry of the CPG, but asymmetric networks can also generate rigid phase patterns via the same ‘quotient network’ mechanism. Figure 5 shows a 5-node network with trivial symmetry; it has one type of node and three types of arrow. The map

$$\begin{aligned} \varphi : \{1, 2, 3, 4, 5\} &\rightarrow \{1, 2, 3, 4\} \\ \varphi(1) = \varphi(5) &= 1 \quad \varphi(2) = 2 \quad \varphi(3) = 3 \quad \varphi(4) = 4 \end{aligned}$$

is a quotient map ([33, Section 10.7]), also called a graph fibration [7], since it preserves node types, arrow types, and input sets up to isomorphism. It therefore supports all types of phase pattern associated with the  $\mathbb{Z}_2 \times \mathbb{Z}_2$  symmetry of Figure 2, subject to the condition that nodes 1 and 5 are synchronous. However, the symmetry group of the 5-node network of Figure 5 is trivial. Specifically, there is precisely one unidirectional arrow of each type, namely  $2 \rightarrow 5$ ,  $3 \rightarrow 5$ , and  $4 \rightarrow 1$ , so the heads and tails of these arrows are fixed by any symmetry. But these account for all five nodes.

In principle, the extra node can cause transverse instability, so the parameter values for which these lifted gaits are stable might differ from those for the original ones. Simulations show that they can be stable for the 5-node network, for suitable parameters. We have not investigated this issue further.

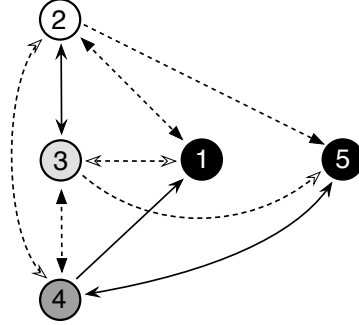


Figure 5: A 5-node lift of Figure 2 with trivial symmetry. The synchrony pattern illustrated, with clusters  $\{1, 5\}$ ,  $\{2\}$ ,  $\{3\}$ ,  $\{4\}$ , determines a quotient network with 4 nodes, isomorphic to Figure 2. Therefore the 5-node network supports the same periodic states (though not necessarily with the same stabilities) as the CPG in Figure 2, but with nodes 1 and 5 are synchronous.

## 1.8 Comparison of Different Neuron Models

Many different types of neuron model have been studied: Boolean switches, Pitts–McCulloch networks, PDEs, integro-differential equations, delay differential equations, stochastic models. . . Surveys and further details can be found in many sources, for example [27, 28, 51, 67, 81, 89, 104]. We comment briefly on five standard types of model neuron that are defined by ODEs.

The first ODE model of a neuron is arguably that of Lapique [61] in 1907. Like many later ones, it was based on an electronic analogy. A biologically more realistic ODE model appeared in the Nobel prizewinning work of Hodgkin and Huxley [49]. The objective was to model the initiation and propagation of action potentials in the giant axon of the longfin inshore squid *Doryteuthis pealeii*, and to obtain a quantitative fit to data obtained from voltage clamp experiments. Their model incorporates ionic mechanisms and is based on cable theory. A major feature was an accurate prediction of the speed of propagation of the nerve impulse. The Hodgkin–Huxley equations are mathematically complex and cumbersome, involving four dynamic variables and numerous parameters, and are best suited for numerical simulation.

To gain insight into key aspects of the dynamics generating a neuron impulse, FitzHugh [23] and Nagumo *et al.* [80] introduced a mathematically simpler model that preserves some key features of the Hodgkin–Huxley model. It is a relaxation oscillator, generalising the classical Van der Pol oscillator. This model has only two variables, making it amenable to standard methods of analysis such as phase-plane diagrams. It provides geometric mechanisms for the activation and deactivation of a single pulse, but it sacrifices quantitative accuracy.

Morris and Lecar [76] proposed an alternative simplification of the Hodgkin–Huxley model to represent voltage clamp experiments on the barnacle *Balanus nubilus*. Like the FitzHugh–Nagumo model, their equation has two dynamic variables.

Hindmarsh and Rose [47] devised yet another simplification of the Hodgkin–Huxley model, designed to represent both single pulses and bursting. It has three dynamic

variables: the membrane potential and two representing transport through ion channels. It allows a more diverse range of dynamic behaviour, including chaos, and provides qualitative versions of the main types of dynamic behaviour found in experiments.

Wilson and Cowan [105] formulated equations for populations of excitatory and inhibitory neurons, whose mathematical formulation is well suited to modelling networks of such neurons. Their model proposes a pair of integro-differential equations for the time-evolution of the numbers of excitatory and inhibitory neurons. A coarse-grained version leads to a type of ODE known as a *rate model* [22], discussed in Section 3. Here the state of each neuron in the network is represented by two dynamic variables. The *activity variable* receives a linear combination of inputs from all other variables, whose coefficients correspond to a weighted adjacency matrix for the network. This combination of inputs is modulated by a sigmoidal gain function. The *fatigue variable* is internal to the neuron, and causes its activity to die down again. See Section 3.

In this paper, as proof of concept, we employ rate models. With the likely exception of Section 3.2 on Liapunov functions, which relies on the specific form of rate model gain functions, similar analyses based on alternative neuron models could be carried out in much the same manner. Indeed, we have done this for a simpler network in [100].

## 1.9 Summary of Paper

Section 2 recalls from [99] the concept of a feedforward lift network. We discuss three examples: a ‘toy’ model to illustrate mathematical features, and two lifts of Figure 2 that generate the same phase patterns as Figure 2 and thus might equally well model biped locomotion while propagating signals along chains of short-range connections. We summarise three notions of stability for periodic orbits — Liapunov, asymptotic, and Floquet stability. We discuss ‘transverse’ versions of these stability conditions, appropriate to feedforward lifts, along with a fourth form of stability: transverse stability of the synchrony subspace. We state three basic stability theorems from [99].

Section 3 specialises the analysis to rate (or Wilson–Cowan) models. A similar analysis could be performed using other neuron models, and [100] suggests that stable travelling waves would be likely. The relevant stability notions are recalled in Section 2.1. First, we show that the synchrony subspace of any rate model is transversely stable. By [73] this does not imply Floquet stability, but it suggests that Floquet stable lifted states should be common. In Section 3.2 we construct two Liapunov functions that ensure transverse Liapunov stability for rate models when parameters lie in specified ranges. One of them also guarantees Floquet stability over a slightly smaller range. We simulate the lifted periodic state numerically for four parameter sets that satisfy the stability conditions, and compute CPG and transverse Floquet multipliers numerically.

Section 4 applies the theory of feedforward lifts and transverse stability to two models of biped locomotion, shown in Figure 3. These models are lifts of the CPG of figure 2 proposed in [87], itself derived from [34, 35]. The lifts propagate phase-synchronous signals along an arbitrarily long chain with only short-range connections. One model uses a feedforward lift to replace the 4-node CPG by an arbitrarily long feedforward chain driven by that CPG, which might be more plausible physiologically. The second model is *almost* a feedforward lift, except for lateral connections. Again, this topology is plausible.

The synchrony subspace for the first model is transversely stable by Theorem 3.2. We give analytic conditions for transverse stability for the second model. We compute transverse eigenvalues numerically along the periodic orbit. We also compute transverse Floquet multipliers and compare these two stability notions.

Finally, we summarise the main conclusions in Section 5.

## 2 Feedforward Lifts

A feedforward lift [99] of a given network is a lift with two components:

- (a) The original network, now referred to as a *CPG*.
- (b) A *chain*, or a more complex branching structure, which receives signals from the CPG but does not send signals to it. Nodes in the chain are connected in a feed-forward (also called ‘acyclic’) manner, and input arrows are arranged so that they receive the same signals as suitable nodes in the CPG.

The formal definition of a feedforward lift is given in [99, Definition 3.4]. We do not repeat it here since the feedforward lifts in this paper are described explicitly. However, it underpins the general stability theorems that we require. The main point of [99] is that any feedforward lift of a given network can propagate time-periodic phase-related signals in a natural manner along a chain or even a branching tree, and these signals are often stable (even to synchrony-breaking perturbations).

**Example 2.1.** Figure 6 is a simple ‘toy’ example used in [99] to illustrate the main ideas, and initially we use it here for simplicity.

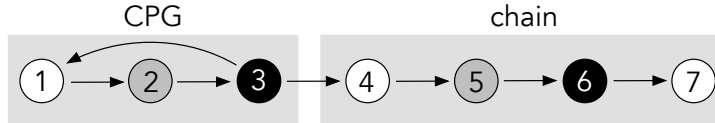


Figure 6: A 7-node network with one node-type and one-arrow type. The colouring (black, grey, white) is balanced. This network naturally propagates signals such that nodes of the same colour are in synchrony, and successive nodes are phase-shifted by  $\frac{1}{3}$  of the period. The CPG  $\{1, 2, 3\}$  has cyclic group symmetry  $\mathbb{Z}_3$ .

The CPG is the subnetwork with nodes  $\{1, 2, 3\}$  and the arrows connecting them; the chain comprises the remainder of the network. Intuitively, nodes 1 and 4 receive the same signal from node 3 and have the same internal dynamics, so they can synchronise. Then nodes 2 and 5 receive synchronous signals, so they can synchronise. Similarly node 6 can synchronise with node 3, node 7 with node 4, and so on for longer chains. More formally, the colouring shown is *balanced*: nodes of the same colour have inputs that are colour-isomorphic. See [33, Chapters 8, 10].

The CPG  $\{1, 2, 3\}$  has cyclic group symmetry  $\mathbb{Z}_3$ , so a natural phase pattern for a period oscillation involves a  $\frac{1}{3}$ -period phase shift between successive nodes [32, 33, 31, 36, 97]. The synchrony pattern ensures that these phase shifts are replicated along the chain. Figure 7 in Section 3.3 shows numerical examples of such phase patterns.

A more complex example of a feedforward lift is shown in Figure 3 (top). The very similar topology of Figure 3 (bottom) is not a feedforward lift in the strict sense, but more general results apply to it. We introduce these two networks because the network of Figure 2 need not be taken literally as the exact CPG architecture for a biped. In particular, *any* lift of that network has the same dynamics when restricted to a suitable synchrony subspace; that is, synchronous clusters have the same waveforms and phase relations as the nodes of the 4-node CPG. So the chains of repeating modules in Figure 3 propagate phase patterns to more distant parts of the animal via exclusively short-range connections. Figure 5 shows a non-feedforward lift, to which similar remarks apply. However, when the lift is feedforward there is a systematic way to analyse stability: [99, Theorem 5.4] shows that in that case, when transverse Floquet multipliers are stable, the patterns concerned have the same stabilities as they do for the CPG. (This is true for each of the main three notions of stability of a periodic state: asymptotic, Liapunov, or Floquet.) Indeed, the lifted dynamics can be stable even when some connections are not feedforward.

Moreover, transverse Floquet stability of the lifted periodic state for one extra ‘module’ in a feedforward lift implies transverse Floquet stability for any number of extra modules. As suggested in [100], this feature may offer evolutionary advantages.

## 2.1 Stability and Transverse Stability

As already mentioned, a crucial issue is the stability of the signals, which is necessary for them to model reasonable biology. In order for a propagating signal created by a feedforward lift to be stable — asymptotically, Liapunov, or Floquet — the original CPG periodic orbit must be stable (in the same sense) to synchrony-preserving perturbations and to synchrony-breaking perturbations. The first condition is equivalent to stability of the periodic orbit within the CPG state space, since for a feedforward lift this can be identified with the synchrony subspace concerned. The second condition can be stated as a form of *transverse stability*, and this condition applies unchanged to all such chains and trees. We summarise these ideas in Section 2.2.

When these stability conditions hold, a feedforward lift propagates phase patterns of periodic states in a robust (indeed, technically ‘rigid’) manner, making them suitable for locomotion models. In [100] we examined four standard neuron models (FitzHugh–Nagumo, Morris–Lecar, Hindmarsh–Rose, and Hodgkin–Huxley) from this point of view, for the ‘toy’ 7-node network of Figure 6, showing numerically that the stability conditions are often satisfied.

The present paper focuses on a fifth type of model: Wilson–Cowan (or rate model) neurons. It has two main aims. One is to prove analytically that such models are transversely stable, either in the sense of Liapunov stability or more strongly Floquet stability, if certain conditions on parameters are satisfied. The other is to study stability if propagating signals for two feedforward lifts for a CPG for biped locomotion introduced in [99]. We use both analytic and numerical methods to do this.

### Three Stability Notions

We recall three stability notions for equilibria and periodic orbits, each stronger than the previous one. For further information see [78, Chapter 4] and [62, 63, 65]. Let  $\|\cdot\|$  be any norm on  $\mathbb{R}^n$ . In this paper we use the Euclidean norm unless otherwise stated. All norms on  $\mathbb{R}^n$  are equivalent.

**Definition 2.2.** Let  $x(t)$  be an orbit of an ODE  $\dot{x} = f(x)$ . Then an equilibrium  $a_0$  is:

(a) *Liapunov stable* if, for every  $\varepsilon > 0$ , there exists  $\delta > 0$  such that if  $\|x(0) - a_0\| < \delta$  then  $\|x(t) - a_0\| < \varepsilon$  for all  $t > 0$ .

(b) *Asymptotically stable* if it is Liapunov stable, and in addition  $\delta$  can be chosen so that  $\|x(t) - a_0\| \rightarrow 0$  as  $t \rightarrow +\infty$ .

(c) *Exponentially stable* if there is a neighbourhood  $V$  of  $a_0$  and constants  $K, \alpha > 0$  such that  $\|x(t) - a_0\| < Ke^{-\alpha t}$  for all  $x(0) \in V$ .

(For some norm, not necessarily the Euclidean one, we can assume  $K = 1$ .)

Exponential stability implies asymptotic stability, which in turn implies Liapunov stability. Neither converse is valid in general. *Linear stability* (all eigenvalues of the Jacobian at  $a_0$  have negative real part) is equivalent to exponential stability [48].

We can transfer these stability conditions to a periodic orbit (trajectory)  $\{a(t)\}$  via a Poincaré map. An alternative, more classical, approach is to define  $y(t) = x(t) - a(t)$ . Then the *system of deviations*

$$\dot{y} = f(y + a(t)) - \dot{a}(t) \tag{2.1}$$

is a non-autonomous ODE with a fixed equilibrium  $y = 0$ . The orbit  $\{a(t)\}$  is defined to be stable, in any of the senses (a), (b), (c) of Definition 2.2, if this equilibrium is stable in the same sense.

Since  $y(t) = x(t) - a(t)$  we can restate the definition for Liapunov stability of an orbit (in particular, a periodic one):

**Definition 2.3.** The orbit  $\{a(t)\}$  is *Liapunov stable* if, for any  $\varepsilon > 0$ , there exists  $\delta > 0$  such that whenever  $\|x(0) - a(0)\| < \delta$  we have  $\|x(t) - a(t)\| < \varepsilon$  for all  $t \geq 0$ .

There are corresponding definitions of asymptotic and exponential stability for orbits. Often these are called orbital asymptotic and exponential stability. Again, exponential stability implies asymptotic stability, which in turn implies Liapunov stability. Exponential stability is equivalent to Floquet stability [48].

### Liapunov Functions

Liapunov stability can sometimes be proved using a *Liapunov function*  $L(x)$ .

**Definition 2.4.** Let  $a_0$  be an equilibrium of an ODE on  $\mathbb{R}^n$ . Then a (local) *Liapunov function* is a map  $L : N \rightarrow \mathbb{R}^n$ , where  $N$  is a neighbourhood of  $a_0$ , such that:

(a)  $L(x) \geq 0$  for all  $x$  near  $a_0$ .

(b)  $L(x) = 0$  if and only if  $x = a_0$ .

A further condition strengthens this notion:

(c)  $\frac{d}{dt}L(x(t)) \leq 0$  for all  $x(0) \in N, t \geq 0$ , where  $x(t)$  is the forward orbit of  $x(0)$ .

A more explicit bound implies exponential stability:

(d) There is a constant  $\alpha > 0$  such that  $\frac{d}{dt}L(x(t)) \leq -\alpha L(x(t))$  for  $t \geq 0$

*Liapunov's Second Method* [62, 63] is the observation that the existence of a Liapunov function satisfying (a), (b), and (c) implies that  $A$  is asymptotically stable. If only (a) and (b) hold, it is Liapunov stable. If (d) also holds, it is exponentially stable.

## Transverse Stability

For an admissible ODE of a feedforward lift, the three notions of stability apply directly to the CPG dynamics, ignoring the chain that it drives. The structure of a feedforward lift implies that the CPG dynamics can be identified naturally with (is ‘conjugate’ to) the dynamics of the corresponding synchronous clusters. We can therefore split the stability conditions into two parts: stability to perturbations that preserve synchrony, and to perturbations that break synchrony. The first part corresponds to stability of the CPG dynamics; the second is what we have called transverse stability.

In [99] we define transverse asymptotic, Liapunov, and Floquet stability for a periodic orbit. The idea is to consider the system of deviations (2.1) and require the corresponding stability condition for the fixed point defined by the periodic orbit  $\{a(t)\}$  and let us focus on the transverse dynamics. Linearising this equation leads to Floquet theory.

We prove that for each of the three types of stability in Definition 2.2, the lifted signal  $\{\tilde{a}(t)\}$  is stable if and only if the periodic orbit  $\{a(t)\}$  of the CPG is stable and it satisfies the corresponding transverse stability condition. We emphasise that this condition depends only on the CPG dynamics, although it differs from stability of  $\{a(t)\}$  itself. This fact is a consequence of the combination of the feedforward structure with the imposed phase pattern.

Transverse Liapunov stability is defined in [99, Section 5.5], and a transverse version of asymptotic stability is also referred to there. It is proved in [99, Theorem 5.4] that the lifted periodic orbit  $\{\tilde{a}(t)\}$  is Floquet stable if and only if  $\{a(t)\}$  is Floquet stable on the CPG state space and  $\{\tilde{a}(t)\}$  is transversely Floquet stable. Analogous results hold for Liapunov and asymptotic stability. We state the relevant theorems in Section 2.2.

## Transverse Stability of the Synchrony Subspace

A different notion of transverse stability is discussed in [99, Section 6]. Here we consider the dynamic transverse to the synchrony subspace at each point. Feedforward structure gives the Jacobian a block-triangular form, with one block for the CPG and diagonal blocks for successive nodes along the chain. The synchrony subspace is *transversely stable* if these diagonal blocks have eigenvalues with negative real parts.

It is tempting to assume that this form of transverse stability should imply transverse Floquet stability. This is true if node spaces are 1-dimensional [99, Theorem 6.4]. However, the Markus-Yamabe counterexample [73] and [99, Example 6.3] show that it is false in general. Despite this, it remains a useful heuristic. We compared transverse stability with transverse Floquet stability in [100] for standard neuron models in the network of Figure 6.

## 2.2 Stability Theorems for Feedforward Lifts

We summarise the main stability results of [99], with minor changes to conform to this paper.

The first [99, Theorem 5.4] is a necessary and sufficient condition for Floquet stability of a feedforward lift:

**Theorem 2.5.** *Let  $\{\tilde{a}(t)\}$  be a feedforward lift of the periodic orbit  $\{a(t)\}$  on the CPG. Then:*

(a) *The Floquet multipliers for  $\{\tilde{a}(t)\}$  are the Floquet multipliers for  $\{a(t)\}$  on the CPG, together with the transverse Floquet multipliers for all nodes of the chain.*

(b) *The transverse Floquet multipliers for any node of the chain are the same as those for a synchronous node in the CPG.*

(c)  *$\{\tilde{a}(t)\}$  is stable on  $P$  if and only if  $\{a(t)\}$  is stable in the CPG state space, and all transverse Floquet multipliers have absolute value  $< 1$  for every node in the CPG.*

The second [99, Theorem 7.1] adds further detail for phase patterns:

**Theorem 2.6.** *Assume that the CPG  $\mathcal{G}$  has nodes  $\mathcal{C} = \{1, \dots, m\}$  with a cyclic automorphism group  $\mathbb{Z}_k = \langle \alpha \rangle$ , such that  $n = mk$  and  $\alpha$  acts like the cycle  $(1\ 2 \dots k)$  on all of its orbits on  $\mathcal{G}$ . Let  $\{a(t)\}$  be a  $T$ -periodic solution of an admissible ODE with discrete rotating wave phase pattern. Choose a set  $\mathcal{M}$  of orbit representatives. Let  $\tilde{\mathcal{G}}$  be obtained by lifting appropriate copies of translates  $\mathcal{M}_{k+1}, \mathcal{M}_{k+2}, \dots, \mathcal{M}_l$  of this set by  $\mathbb{Z}_k$ . Then*

(a) *The periodic state  $\{a(t)\}$  on  $\mathcal{G}$  lifts to a  $T$ -periodic travelling wave state  $\{\tilde{a}(t)\}$  for  $\tilde{\mathcal{G}}$  with phases corresponding to the copies  $\mathcal{M}_{k+1}, \mathcal{M}_{k+2}, \dots, \mathcal{M}_l$  of  $\mathcal{M}$ .*

(b) *The Floquet exponents of  $\{\tilde{a}(t)\}$  (evaluated at any point) are those on the module  $\mathcal{M}$ , together with the transverse Floquet exponents for  $\mathcal{M}$ .*

(c) *If the Floquet exponents and the transverse Floquet exponents on  $\mathcal{M}$  have negative real part, then  $\{\tilde{a}(t)\}$  is stable.*

The third [99, Theorem 5.10] is an analogous result for Liapunov stability:

**Theorem 2.7.** *The lifted periodic orbit  $\{\tilde{a}(t)\}$  is Liapunov stable if and only if  $\{a(t)\}$  is Liapunov stable in the CPG state space and transversely Liapunov stable.*

There is a natural analogue of Theorem 2.6(c) for Liapunov stability, proved in the same manner. We do not state it here.

**Remark 2.8.** If network  $\mathcal{G}$  is a lift of network  $\mathcal{H}$  then *all* dynamic states for  $\mathcal{H}$  are preserved (subject to the appropriate synchrony pattern) when lifted to  $\mathcal{G}$ , not just equilibria and periodic states. However, the concept of stability is more complicated for more complex states such as chaos. Indeed, stability on the CPG alone is more complicated, because there are many different concepts of an ‘attractor’ [75]. Transverse stability opens up further complications, and is mainly understood for discrete dynamics and only one transverse dimension [4, 5], and even then there are several different scenarios. Synchronous chaos is important as one method to ensure secure communications, and has been widely studied from an electronic engineering viewpoint, see for example [84, 85, 86].

### 3 Rate Models

Having motivated the notion of a feedforward lift, and set up the theoretical aspects that we require, we now discuss stability properties of lifted periodic orbits in three specific feedforward lifts: the 7-node network of Figure 6 and the two proposed networks for biped locomotion in Figure 2.

We model the dynamics of each node using a *rate model*, also called a *Wilson–Cowan* model [22]. Here each node represents a neuron (or a population of neurons), and the node variables correspond to the rate at which the neuron fires. The state of node  $\mathcal{N}_i$  is described by a two-variable vector  $x_i = (x_i^E, x_i^H)$ , where  $x_i^E \in \mathbb{R}$  is an *activity variable* and  $x_i^H \in \mathbb{R}$  is a *fatigue variable*.

Nodes are coupled through a *gain function*  $\mathcal{G} : \mathbb{R} \rightarrow \mathbb{R}$ . This satisfies the following conditions:

- (1)  $0 \leq \mathcal{G}(x) \leq \rho$  for all  $x \in \mathbb{R}$  and for some  $0 < \rho \in \mathbb{R}$ .
- (2)  $0 \leq \mathcal{G}'(x) \leq \sigma$  for all  $x \in \mathbb{R}$  and for some  $0 < \sigma \in \mathbb{R}$ .
- (3)  $\lim_{x \rightarrow -\infty} \mathcal{G}(x) = 0$  and  $\lim_{x \rightarrow +\infty} \mathcal{G}(x) = \rho$ .
- (4)  $\mathcal{G}(x) \approx 0$  when  $x \leq 0$ .

Usually  $\mathcal{G}$  is sigmoid, so there is a unique inflexion point  $x_0$  where  $\mathcal{G}''(x_0) = 0$ , but we do not make this a requirement.

A standard choice of gain function is

$$\mathcal{G}(x) = \frac{a}{1 + e^{-b(x-c)}} \quad (3.2)$$

where  $a, b, c > 0$ . (This notation is employed here for consistency with the literature and should not be confused with other uses in this paper.) See [60, 93] for a discussion of such models in the context of binocular rivalry. With reasonable choices of  $a, b, c$  the value of  $\mathcal{G}(x)$  is very small when  $x \leq 0$ . A standard choice in the literature is  $a = 0.8, b = 7.2, c = 0.9$ , for which  $k = 0.8$ . In the simulations of Section 4.2 we use similar but simpler parameters. Note that although  $\mathcal{G}(x)$  is very small for negative  $x$ , it is not identically zero. Thus a ‘passive’ node might not have a state exactly equal to zero; instead, its values will be very close to zero. This assumption is convenient for programming simulations and is standard in the literature.

The node equations are specified in terms of a *connection matrix*

$$A = (\alpha_{ij}) \quad 1 \leq i, j \leq n$$

where  $n$  is the number of nodes, and  $\alpha_{ij}$  is the strength of the connection from node  $j$  to node  $i$  (positive for excitation, negative for inhibition). The equations take the form

$$\begin{aligned} \varepsilon \dot{x}_i^E &= -x_i^E + \mathcal{G} \left( -gx_i^H + \sum_{j \neq i} \alpha_{ij} x_j^E + I_i \right) \\ \dot{x}_i^H &= x_i^E - x_i^H \end{aligned} \quad (3.3)$$

for  $1 \leq i \leq n$ . This is a fast-slow system, and  $\varepsilon \ll 1$  is the timescale on which  $x_i^E$  evolves. The parameter  $g > 0$  is the strength of reduction of the activity variable by the fatigue variable.  $I_i$  is the external signal strength to node  $i$ . For simplicity it is standard to let  $I_i = 0$  if node  $i$  is inactive, and  $I_i = I$  if node  $i$  is active, for a constant  $I$  usually taken to equal 1. However, we consider the general case here.

### 3.1 Transverse Stability for Rate Models

Rate models have 2-dimensional node spaces, so [99, Theorem 6.4] does not apply. Nonetheless, we can state and prove several theorems giving conditions under which lifted periodic states for a rate model are transversely stable, transversely Liapunov-stable, or transversely Floquet-stable.

The simplest (but least useful) case is transverse stability. We prove that all rate models are transversely stable. As noted at the end of Section 2.1, this does not imply Floquet-stability of lifted periodic orbits, but it suggests that Floquet-stability is likely.

The following lemma is well known and easy to prove:

**Lemma 3.1.** *All eigenvalues of a  $2 \times 2$  matrix  $A$  have negative real part if and only if  $\text{tr}(A) < 0$  and  $\det(A) > 0$ .  $\square$*

We immediately deduce:

**Theorem 3.2.** *For any rate model and any feedforward lift, the synchrony space  $S$  is transversely stable at every point.*

*Proof.* The diagonal part of the Jacobian, for node  $i$ , is equal to

$$A = \begin{bmatrix} -1/\varepsilon & -\frac{g}{\varepsilon} \mathcal{G}' \left( -gx_i^H + \sum_{j \neq i} \alpha_{ij} x_j^E + I_i \right) \\ 1 & -1 \end{bmatrix} \quad (3.4)$$

Therefore

$$\begin{aligned} \text{tr}(A) &= -1/\varepsilon - 1 < 0 \\ \det(A) &= 1/\varepsilon + \frac{g}{\varepsilon} \mathcal{G}' \left( -gx_i^H + \sum_{j \neq i} \alpha_{ij} x_j^E + I_i \right) > 0 \end{aligned}$$

because  $\varepsilon > 0$  and  $\mathcal{G}'(x) \geq 0$  for all  $x$ . Now apply Lemma 3.1.  $\square$

For this reason we do not show plots of the real parts of transverse eigenvalues for the rate models considered below.

### 3.2 Liapunov Functions for Rate Models

In this section we construct two Liapunov functions for rate models, which show that under certain conditions on parameters, lifted periodic states are transversely Liapunov stable. By condition (c) of Definition 2.4, the same Liapunov function implies transverse

asymptotic stability. With some extra effort we can use condition (d) of Definition 2.4 to parlay this result into a proof of transverse Floquet-stability under slightly different conditions. It is probably possible to improve on these results. They can be viewed as proof-of-concept; we apply them to a model of biped locomotion in Section 4.7.

To simplify expressions, scale time from  $t$  to  $s = \varepsilon t$ . Then  $ds = \varepsilon dt$  so  $d/ds = \frac{1}{\varepsilon}d/dt$ . In scaled time (now called  $t$ ) we can write the Floquet equation for transverse stability as

$$\begin{bmatrix} \dot{u} \\ \dot{v} \end{bmatrix} = \begin{bmatrix} -1 & -g\eta(t) \\ \varepsilon & -\varepsilon \end{bmatrix} \begin{bmatrix} u \\ v \end{bmatrix}$$

where  $\eta(t)$  is the input to the first node  $c$  of the chain from the CPG:

$$\eta(t) = \mathcal{G}' \left( -gx_{[c]}^H(t) + \sum_{j \neq i} \alpha_{ij} x_{[j]}^E(t) + I_i \right) \geq 0 \quad \text{for all } t \in \mathbb{R} \quad (3.5)$$

Here  $[c]$  is the node in the CPG that is synchronous with node  $c$ .

In fact,  $\eta(t) > 0$  for all  $t \in \mathbb{R}$  for the gain function (3.2). Since a periodic orbit is compact, there exist bounds  $D_0, D$  such that

$$0 \leq D_0 \leq \eta(t) \leq D \quad (3.6)$$

and  $g, \varepsilon \geq 0$ . For the gain function (3.2) we have  $D_0 > 0$ . Define

$$\zeta(t) = g\eta(t) \geq 0$$

and when  $t$  is irrelevant write  $\zeta$  in place of  $\zeta(t)$ . Then

$$0 \leq \zeta(t) \leq gD$$

### Liapunov Function 1

The function  $\sqrt{\varepsilon x^2 + y^2}$  is a norm on  $\mathbb{R}^2$ . We claim that

$$L(t) = \varepsilon u^2 + v^2$$

is a Liapunov function provided  $-1 < \zeta < 3$ .

**Remark 3.3.** The norm itself is also a Liapunov function under the same conditions. Indeed,

$$\frac{d}{dt} \sqrt{\varepsilon u(t)^2 + v(t)^2} = \frac{\frac{d}{dt}(\varepsilon u(t)^2 + v(t)^2)}{2\sqrt{\varepsilon u(t)^2 + v(t)^2}}$$

so this norm of  $(u(t), v(t))$  is a Liapunov function provided  $L(t)$  is. We work with  $L(t)$  for simplicity.

We have:

$$\begin{aligned} \dot{L}(t) &= 2\varepsilon u\dot{u} + 2v\dot{v} \\ &= 2\varepsilon u(-u - \zeta v) + 2v\varepsilon(u - v) \end{aligned}$$

so

$$\begin{aligned}
-\frac{1}{2}\dot{L}(t) &= \varepsilon u(u + \zeta v) + v\varepsilon(-u + v) \\
&= \varepsilon u^2 + (\zeta\varepsilon - \varepsilon)uv + \varepsilon v^2 \\
&= \varepsilon(u^2 + (\zeta - 1)uv + v^2)
\end{aligned}$$

We seek regions in which  $u^2 + (\zeta - 1)uv + v^2 \geq 0$ . Then  $\dot{L}(t) \leq 0$  so  $L(t)$  is a Liapunov function.

To make the quadratic form  $Q(u, v) = u^2 + (\zeta - 1)uv + v^2$  positive definite, consider its discriminant

$$\Delta = (\zeta - 1)^2 - 4 = \zeta^2 - 2\zeta - 3$$

This is negative when  $-1 < \zeta < 3$ . Now  $\Delta < 0$  implies that  $Q$  is definite, and it is clearly positive definite (since when  $\zeta = 1$ , inside that range, it is  $u^2 + v^2$ ).

This proves:

**Proposition 3.4.** *If  $0 \leq gD \leq 3$  then the lifted periodic orbit  $\{\tilde{a}(t)\}$  is transversely Liapunov stable.  $\square$*

With a little more effort we can prove transverse Floquet stability:

**Proposition 3.5.** *If  $\varepsilon \leq 4$  and  $0 \leq gD_0 < \frac{1}{2}(2 + \sqrt{3(4 - \varepsilon)})$ , the lifted periodic orbit  $\{\tilde{a}(t)\}$  is transversely Floquet stable.*

*Proof.* We use condition (d) in Section 2.1. Suppose we can obtain a more specific estimate of the form

$$\dot{L}(t) \leq -kL(t) < 0 \quad \text{or equivalently,} \quad \dot{L}(t) + kL(t) < 0$$

for some  $k > 0$ . Then we deduce that  $L(t) \leq Ke^{-kt}$  for a constant  $K$ , which tends exponentially to 0. This proves transverse exponential stability, which is equivalent to Floquet stability.

In particular, this condition holds if  $k = gD_0$  for  $D_0$  as in (3.6). (We need  $D_0$ , not  $D$ , because of the minus sign. Recall from (3.5) that  $\eta(t) \geq 0$  for all  $t \in \mathbb{R}$ .)

To obtain such a constant  $k$ , consider

$$\begin{aligned}
\dot{L}(t) + kL(t) &= -2\varepsilon(u^2 + (\zeta - 1)uv + v^2) + k(\varepsilon u^2 + v^2) \\
&= u^2(-2\varepsilon + k\varepsilon) + 2uv\varepsilon(\zeta - 1) + v^2(-2\varepsilon + k)
\end{aligned}$$

Let  $k = \varepsilon/2$ . Then

$$\begin{aligned}
\dot{L}(t) + kL(t) &= u^2(-2\varepsilon + \varepsilon^2/2) + 2uv\varepsilon(\zeta - 1) + v^2(-\frac{3}{2}\varepsilon) \\
&= -[u^2(2\varepsilon - \varepsilon^2/2) + 2uv\varepsilon(1 - \zeta) + v^2(\frac{3}{2}\varepsilon)]
\end{aligned}$$

We seek to make the quadratic form

$$Q(u, v) = u^2(2\varepsilon - \varepsilon^2/2) + 2uv\varepsilon(1 - \zeta) + v^2(\frac{3}{2}\varepsilon)$$

positive definite. Then the minus sign makes  $\dot{L}(t) + kL(t) \leq 0$  as required.

The discriminant of Q is

$$\Delta = 4\varepsilon^2(1 - \zeta)^2 - 4(2\varepsilon - \varepsilon^2/2)(\frac{3}{2}\varepsilon) = \varepsilon^2(4\zeta^2 - 8\zeta - 8 + 3\varepsilon)$$

For arbitrary  $\varepsilon > 0$  the zeros of  $\Delta$  are  $\frac{1}{2}(2 \pm \sqrt{3(4 - \varepsilon)})$ . These are real whenever  $\varepsilon \leq 4$ . When  $\varepsilon$  lies between these zeros,  $\Delta < 0$ .  $\square$

**Example 3.6.** When  $\varepsilon = 0.5$ ,  $\Delta$  is negative whenever  $-0.224745 \leq \zeta \leq 2.22474$ . With  $\varepsilon = 0.6$  it is negative whenever  $-0.596872 \leq \zeta \leq 2.59687$ .

As  $\varepsilon \rightarrow 0$  the bounds  $\frac{1}{2}(2 \pm \sqrt{3(4 - \varepsilon)})$  tend to  $1 \pm \sqrt{3} = 2.73205, -.73205$ .  $\diamond$

## Liapunov Function 2

The function  $\sqrt{\varepsilon^2 x^2 + y^2}$  is also a norm on  $\mathbb{R}^2$ . Let

$$L(t) = \varepsilon^2 u(t)^2 + v(t)^2$$

Then

$$-\frac{1}{4}\dot{L}(t) = \varepsilon^2 u^2 + (\zeta\varepsilon^2 - \varepsilon)uv + \varepsilon v^2 = \varepsilon(\varepsilon u^2 + (\zeta\varepsilon - 1)uv + v^2)$$

If  $\varepsilon u^2 + (\zeta\varepsilon - 1)uv + v^2 \geq 0$ , then  $\dot{L}(t) \leq 0$  so  $L(t)$  is a Liapunov function. We seek regions in which this condition holds.

To make the quadratic form  $Q(u, v) = \varepsilon u^2 + (\zeta\varepsilon - 1)uv + v^2$  positive definite, consider its discriminant

$$\Delta = \varepsilon^2[(\varepsilon\zeta - 1)^2 - 4\varepsilon]$$

Again  $\Delta < 0$  implies that  $Q$  is definite, and it is clearly positive definite. This happens when

$$\frac{1 - 2\varepsilon}{\varepsilon} < \zeta < \frac{1 + 2\varepsilon}{\varepsilon}$$

If, for example,  $\varepsilon = 0.5$ , this is negative when  $-0.828427 \leq \zeta \leq 4.82843$ .

If, for example,  $\varepsilon = 0.6$ , this is negative when  $-0.596872 \leq \zeta \leq 2.59687$ .

This proves:

**Proposition 3.7.** *If  $0 \leq gD \leq 4.82843$  and  $\varepsilon = 0.5$ , then the lifted periodic orbit is transversely Liapunov stable for  $t \geq 0$ .*  $\square$

Estimates like this can be obtained for a variety of similar functions  $L(t)$ . Since the above results are ‘proof of concept’, we do not seek more general statements.

## 3.3 Simulations for 7-Node Chain

Propositions 3.4 and 3.5 apply only to *transverse* stability (in the Liapunov or Floquet sense). For stability of the lifted periodic state we also require the CPG periodic state to be stable. We currently have no analytic results about this issue, but we present some numerical computations of both CPG and transverse Floquet multipliers.

In this subsection we investigate a rate model for the 7-node chain, of the form

$$\begin{aligned}\varepsilon \dot{x}_i^E &= -x_i^E + \mathcal{G}\left(-gx_i^H + \alpha x_{c(i)}^E + I\right) \\ \dot{x}_i^H &= x_i^E - x_i^H\end{aligned}\tag{3.7}$$

for  $1 \leq i \leq 7$ . Here  $c(i) = i - 1$  when  $i > 1$ , and  $c(1) = 3$ . We use the gain function

$$\mathcal{G}(x) = \frac{1}{1 + e^{-8(x-1)}} = \frac{1}{1 + e^{8(1-x)}}\tag{3.8}$$

from [94, Section 14].

For a wide range of parameters leading to the travelling wave with  $\frac{1}{3}$ -period phase shifts, the computed transverse Floquet exponents indicate stability. Table 2 shows CPG and transverse Floquet multipliers for the 7-node chain with 3-node CPG, for the four parameter sets listed in (3.9–3.12). As is well known [44, Section 1.5], the Floquet operator always has at least one multiplier equal to 1, corresponding to an eigenvector tangent to the orbit. This multiplier occurs on the CPG, but not among the transverse multipliers.

param.	$T$	CPG multipliers	abs.	transverse multipliers	abs.
(3.9)	5.783	1	1	0.546	0.546
stable		$0.433 \pm 0.181 i$	0.470	0.00315	0.00315
		0.396	0.396		
		0.0368	0.0368		
		$1.58 \times 10^{-6}$	$1.58 \times 10^{-6}$		
(3.10)	4.612	1	1	0.0898	0.0898
stable		$0.0326 \pm 0.0934 i$	0.0989	0.0110	0.0110
		$0.021 \pm 0.0372 i$	0.0428		
		0.0000538	0.0000538		
(3.11)	3.146	1	1	$0.0199 \pm 0.150 i$	0.151
stable		$0.484 \pm 0.207 i$	0.526		
		0.419	0.419		
		0.0578	0.0578		
		0.00178	0.00178		
(3.12)	4.373	1	1	0.0260	0.0260
stable		$-0.0120 \pm 0.0269 i$	0.0294	0.0146	0.0146
		0.0138	0.0138		
		$-0.000996 \pm 0.00190 i$	0.00215		

Table 2: CPG and transverse Floquet multipliers for the four rate model examples. The CPG periodic orbit and the lifted periodic orbit are stable for all four parameter sets. All entries stated to three significant figures after the decimal point.

Figure 7 shows the corresponding time series for the three different synchrony classes.

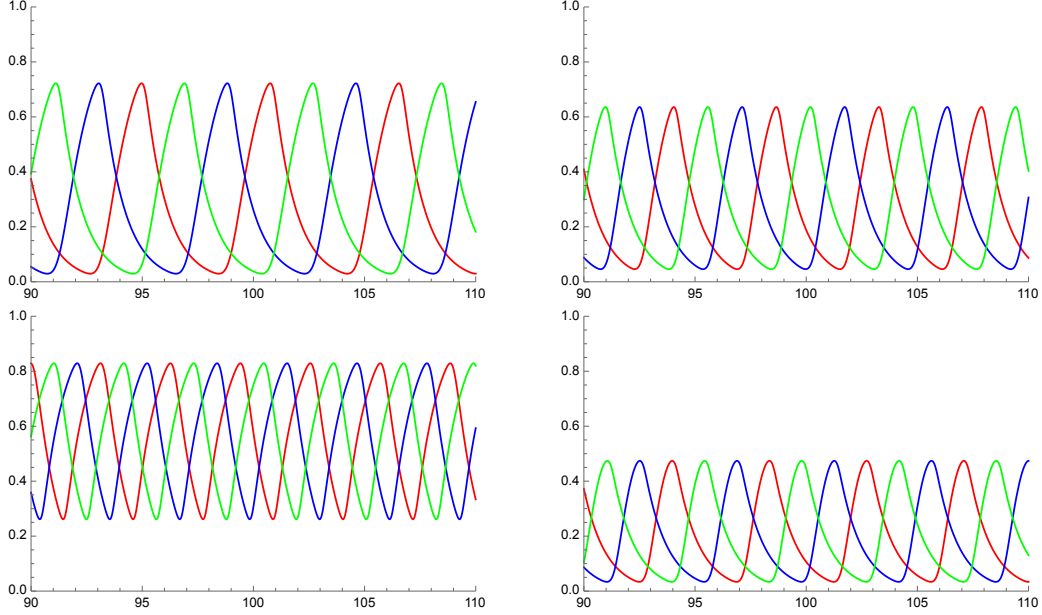


Figure 7: Simulated time series for  $x_1^E, x_2^E, x_3^E$  for the 7-node chain. Parameter sets are (top left) (3.9), (top right) (3.10), (bottom left) (3.11), (bottom right) (3.12).

We consider four typical parameter sets:

$$I = 2 \quad \alpha = -5 \quad g = 2 \quad \varepsilon = .1 \quad (3.9)$$

$$I = 2 \quad \alpha = -5 \quad g = 2 \quad \varepsilon = .5 \quad (3.10)$$

$$I = 4 \quad \alpha = -3 \quad g = 2 \quad \varepsilon = .2 \quad (3.11)$$

$$I = 2 \quad \alpha = -8 \quad g = 3 \quad \varepsilon = .8 \quad (3.12)$$

**Remark 3.8.** Conditions for a given primary biped gait of the 4-node CPG to be the ‘first bifurcation’, hence potentially Floquet-stable, are given in [94]. Because the symmetry group  $\mathbb{Z}_2 \times \mathbb{Z}_2$  is abelian, the isotropy subgroup acts either trivially (for the hop) or as  $\mathbb{Z}_2$  (run, jump, walk) when the kernel of the action is factored out. Therefore the usual stability criterion for generic Hopf bifurcation applies: a supercritical branch is stable and a subcritical branch is unstable. See [46, Chapter 1 Section 2 Theorem III].

The simulations clearly indicate that the Hopf branches are supercritical near bifurcation, because the phase patterns do not depend on randomly chosen initial conditions. It would be of interest to confirm this analytically, which should be a feasible calculation.

## 4 Application to Biped Locomotion

We now introduce a feedforward lift and a modified version of it, slightly relaxing the feedforward condition, which provides a reasonable model for locomotion of animals with many segments, such as centipedes, millipedes, worms, snakes, and lampreys. Something similar may happen in the spinal column of mammals and reptiles.

We start with the 4-node network of Figure 2, proposed in [87] as a CPG for bipedal locomotion. Each leg corresponds to two nodes: one flexor and one extensor. Figure 3 shows two possible lifts, for the balanced colouring shown in shades of white and grey. The top one is a feedforward lift. The second is not totally feedforward because of the lateral connections, such as those between nodes 5 and 7, or 6 and 8, but similar ideas apply with minor modifications.

Theorem 2.6 applies directly to the top network. Therefore, if the periodic orbit of the CPG is Floquet-stable and the lifted orbit is transversely Floquet-stable, the lifted periodic orbit is Floquet-stable. Figure 3 (bottom) is perhaps more plausible biologically, because the extra nodes in the cascade are grouped into modules with the same architecture, with nearest-neighbour coupling between modules. Each module comprises two nodes with bidirectional connections; such connections are said to be *lateral*. Examples of such modules are  $\{5, 7\}$  and  $\{6, 8\}$ . The CPG has much the same architecture as each module, except that the CPG has four arrows pointing towards the left (upstream). The structure can be continued arbitrarily far, providing a simple way to propagate the oscillation patterns. (The total number of columns can be odd or even.) It would be easy for this kind of network to evolve in an organism such as an arthropod, from which most modern vertebrates evolved.

Figure 3 (bottom) is reminiscent of the network in the nervous system that controls the heartbeat of the medicinal leech, Figure 4. It is very much in the spirit of experimentally observed CPGs [101, 41, 53, 38, 43]. It is also similar to the models studied in [54, 55, 56, 57], but these papers mainly look at continuum limits.

Apart from the shaded square of four nodes (which reproduce Figure 2) no arrows point towards the left, so it is *almost* a feedforward network. However, because there are bidirectional *lateral* connections (dashed arrows, vertical in the figure), Theorem 3.2 does not apply directly. Since these lateral connections are biologically plausible we consider this generalisation in its own right, using similar methods. We will show that transverse stability of the synchrony subspace can occur in a rate model for this network, but it is not valid for all coupling strengths. Transverse Liapunov and Floquet stability also occur for suitable parameters.

## 4.1 Rate Equations for 4-node CPG

First, we consider the 4-node CPG of Figure 2. Following [94], explicit rate equations for this CPG (written in a convenient order in which the activity variables and fatigue variables are collected together) are:

$$\begin{aligned}
\varepsilon \dot{x}_1^E &= -x_1^E + \mathcal{G}(I - gx_1^H + \alpha x_4^E + \beta x_3^E + \gamma x_2^E) \\
\varepsilon \dot{x}_2^E &= -x_2^E + \mathcal{G}(I - gx_2^H + \alpha x_3^E + \beta x_4^E + \gamma x_1^E) \\
\varepsilon \dot{x}_3^E &= -x_3^E + \mathcal{G}(I - gx_3^H + \alpha x_2^E + \beta x_1^E + \gamma x_4^E) \\
\varepsilon \dot{x}_4^E &= -x_4^E + \mathcal{G}(I - gx_4^H + \alpha x_1^E + \beta x_2^E + \gamma x_3^E) \\
\dot{x}_1^H &= x_1^E - x_1^H \\
\dot{x}_2^H &= x_2^E - x_2^H \\
\dot{x}_3^H &= x_3^E - x_3^H \\
\dot{x}_4^H &= x_4^E - x_4^H
\end{aligned} \tag{4.13}$$

Here the parameters are:

- $\alpha$  = strength of *diagonal* connection
- $\gamma$  = strength of *medial* connection
- $\beta$  = strength of *lateral* connection
- $\varepsilon$  = fast/slow dynamic timescale
- $g$  = strength of reduction of activity variable by fatigue variable
- $I$  = input

See Figure 2.

The dynamics and bifurcations of (4.13) are studied in [94]. Despite the nonlinear form of the equations, much of the bifurcation behaviour can be derived analytically. The only local bifurcation from a fully synchronous steady state that can lead to stable states near the bifurcation point is the ‘first bifurcation’. Here either one real eigenvalue passes through zero while the others have negative real part, or a complex conjugate pair of eigenvalues crosses the imaginary axis while the others have negative real part. These bifurcations are, respectively, steady-state (leading to a branch of equilibria) and Hopf (leading to a branch of periodic states). It turns out to be possible to find explicit conditions on the connection strengths  $\alpha, \beta, \gamma$  that ensure that the first local bifurcation leads either to one of four symmetry types of steady-state bifurcation, or one of the four symmetry types of Hopf bifurcation—the four primary gaits. It is also possible to identify explicitly the region of  $(\alpha, \beta, \gamma)$ -space in which no local bifurcations occur. Here the synchronous steady state remains stable and changes continuously whatever value  $I$  takes. This region corresponds to small values of the connection strengths.

The argument of the gain function in (4.13) is a linear combination of state variables. This implies that the four regions of  $(\alpha, \beta, \gamma)$ -space corresponding to primary gaits are connected polyhedra. Each is a truncated pyramid with an equilateral triangle as base. They are congruent, and together they form a hollow regular tetrahedron centred at the origin, Figure 8(left). This is the complement of a small tetrahedron  $\mathcal{T}_*$  in a larger tetrahedron  $\mathcal{T}^*$ : formulas for the coordinates of their vertices can be found in [94].

The four primary gait regions are relatively large when  $K$  is significantly greater than  $k$ . This is the case for reasonable values of the connection strengths and other parameters in the model, so the structure provides a robust way to select specific gait patterns.

Diekman *et al.* [19] analyse rate models in a network with the same symmetry group  $\mathbb{Z}_2 \times \mathbb{Z}_2$  in a model of binocular rivalry. They assume a more general form of the gain function, but take  $\beta = 0, \gamma < 0$  because some connections in their model are always inhibitory.

## 4.2 Simulations

The four primary biped gaits in Table 1 are observed numerically in the rate model (4.13); see [94, Section 14]. The gain function used there is (3.2). For simplicity, that paper assumes values  $a = 1, b = 8, c = 1$  in simulations, and we do the same here for

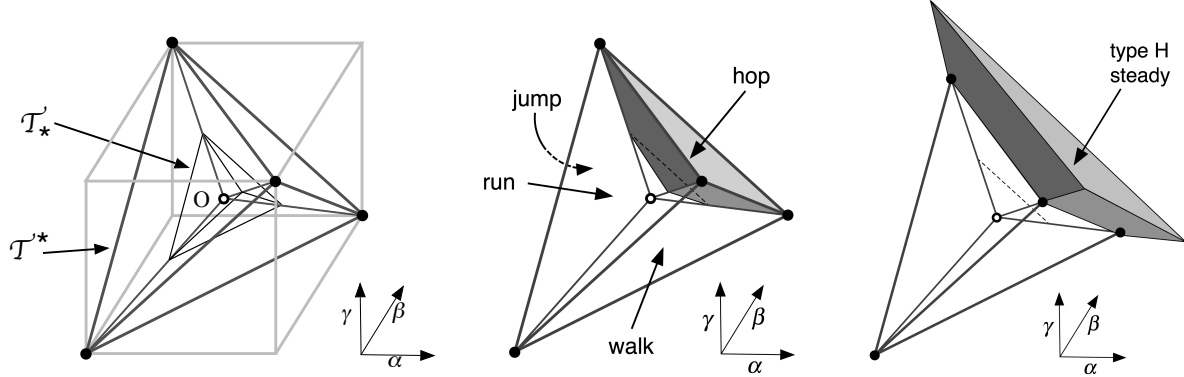


Figure 8: Tetrahedral partition of  $(\alpha, \beta, \gamma)$ -space. *Left:* The two tetrahedra  $\mathcal{T}^*, \mathcal{T}_*$ . *Middle:* Region leading to the hop gait. Base triangle left unshaded to show interior. *Right:* Extending the pyramid to define the corresponding steady-state regions, which extend to infinity in the direction indicated.

consistency. Thus we take

$$\mathcal{G}(x) = \frac{1}{1 + e^{-8(x-1)}} = \frac{1}{1 + e^{8(1-x)}} \quad (4.14)$$

We now consider the corresponding lifted states for the two networks of Figure 3. In particular, we discuss transverse Floquet multipliers for parameter values that yield each primary gait.

### Synchrony and Phase Patterns

We simulated the networks of Figure 3 for a single additional module, using the parameter values of [94, Section 14] used to obtain Figures 19 (hop), 20 (run), 21 (jump), and 22 (walk) of that paper. In all cases the results were identical to those of the CPG alone, with the synchrony or phase pattern propagating correctly to the second module.

As explained in [99, Section 4.4], if the lifted periodic state is stable for one extra module then it is stable for an arbitrary number of extra modules. Since the periodic oscillations observed in numerical experiments, and their synchrony patterns, are robust to changes in initial conditions, we expect them to be stable. Thus the simulation for one extra module indicates stability for any number of extra modules. The computed Floquet multipliers in Tables 3 and 4 confirm this for the parameters stated there.

## 4.3 Transverse Eigenvalues

We now consider the transverse eigenvalues for the two networks in Figure 3.

### Transverse Eigenvalues, 1-Node Module

Figure 3 (top) is a genuine feedforward lift. By Theorem 3.2, all transverse eigenvalues have negative real parts. The same caveat concerning implications for Floquet stability applies.

## Transverse Eigenvalues, 2-Node Module

Theorem 3.2 does not apply to Figure 3 (bottom). As observed earlier, it is enough to consider the transverse eigenvalues for the module  $\{5, 7\}$ .

This network is not a feedforward lift according to [99, Definition 3.4] because  $\tilde{\mathcal{G}}$  contains length-2 loops (the lateral connections) that are not in  $\mathcal{G}$ . However, a similar result holds provided we replace the diagonal block by a block corresponding to a *pair* of laterally connected nodes. For this calculation number those nodes as 1, 2. Note that each node state space is 4-dimensional, so we are working with a  $4 \times 4$  matrix.

The equations for these two nodes are:

$$\begin{aligned}\dot{x}_1^E &= -\frac{1}{\varepsilon}x_1^E + \frac{1}{\varepsilon}\mathcal{G} \left( -gx_1^H + \sum_{j \neq i} \alpha_{1j}x_j^E + I_1 \right) \\ \dot{x}_2^E &= -\frac{1}{\varepsilon}x_2^E + \frac{1}{\varepsilon}\mathcal{G} \left( -gx_2^H + \sum_{j \neq i} \alpha_{2j}x_j^E + I_2 \right) \\ \dot{x}_1^H &= x_1^E - x_1^H \\ \dot{x}_2^H &= x_2^E - x_2^H\end{aligned}$$

where we have grouped activity variables and fatigue variables together, which simplifies the calculation of eigenvalues.

The Jacobian is:

$$J = \begin{bmatrix} -\frac{1}{\varepsilon} & \frac{h}{\varepsilon}G_1 & -\frac{g}{\varepsilon}G_1 & 0 \\ \frac{h}{\varepsilon}G_2 & -\frac{1}{\varepsilon} & 0 & -\frac{g}{\varepsilon}G_2 \\ 1 & 0 & -1 & 0 \\ 0 & 1 & 0 & -1 \end{bmatrix}$$

where

$$\begin{aligned}G_1 &= \mathcal{G}' \left( -gx_1^H + \sum_{j \neq i} \alpha_{1j}x_j^E + I_1 \right) \\ G_2 &= \mathcal{G}' \left( -gx_2^H + \sum_{j \neq i} \alpha_{2j}x_j^E + I_2 \right) \\ h &= a_{12} = a_{21}\end{aligned}$$

Therefore

$$\varepsilon J = \begin{bmatrix} -1 & hG_1 & -gG_1 & 0 \\ hG_2 & -1 & 0 & -gG_2 \\ \varepsilon & 0 & -\varepsilon & 0 \\ 0 & \varepsilon & 0 & -\varepsilon \end{bmatrix}$$

Since this is a  $4 \times 4$  matrix, a *necessary* condition for all eigenvalues to have negative real part is that the trace is negative and the determinant is positive. Calculations show that

$$\begin{aligned}\text{tr}(\varepsilon J) &= -2 - 2\varepsilon < 0 \\ \det(\varepsilon J) &= \varepsilon^2[(1 + gG_1)(1 + gG_2) - h^2G_1G_2]\end{aligned}$$

so the trace is always negative. However, the determinant is positive if and only if

$$h^2 < \left(g + \frac{1}{G_1}\right) \left(g + \frac{1}{G_2}\right)$$

so

$$|h| < \sqrt{\left(g + \frac{1}{G_1}\right) \left(g + \frac{1}{G_2}\right)} \quad (4.15)$$

In other words: strong lateral coupling leads to transverse instability.

As parameters vary continuously, an eigenvalue goes unstable if and only if  $\det J = 0$ . Since  $\varepsilon \neq 0$ , this occurs if and only if

$$(1 + gG_1)(1 + gG_2) - h^2G_1G_2 = 0$$

That is,

$$h = \sqrt{\left(g + \frac{1}{G_1}\right) \left(g + \frac{1}{G_2}\right)} \quad (4.16)$$

Therefore the synchrony subspace is stable transversely whenever (4.15) holds. The determinant argument above shows that it is unstable whenever

$$h > \sqrt{\left(g + \frac{1}{G_1}\right) \left(g + \frac{1}{G_2}\right)}$$

Therefore (4.16) determines the boundary between transverse stability and instability of the synchrony subspace.

### Transverse Jacobians

For comparison, we also computed the eigenvalues of  $J$  numerically for each primary gait, using the parameter values of Figures 19–22 for the hop, run, jump, and walk gaits respectively. All transverse eigenvalues (that is, the eigenvalues of  $J$ ) are negative on the periodic orbit, see Figure 9.

In these figures the real parts of complex conjugate pairs coincide, giving only two values. The small ovals in ‘hop’ correspond to real eigenvalues. All other eigenvalues are complex. Figure 10, which plots the imaginary parts of the eigenvalues, confirms these statements: only the ‘hop’ figure exhibits (short) intervals of zero imaginary part, whose position matches the ovals in the real part.

## 4.4 CPG Floquet Multipliers

We computed the Floquet multipliers for the CPG, for the four gaits *hop*, *run*, *jump*, *walk*, using the parameter values of [94]. For all gaits we take  $a = 1$ ,  $b = 8$ ,  $c = 1$ ,  $\varepsilon = 0.67$ ,

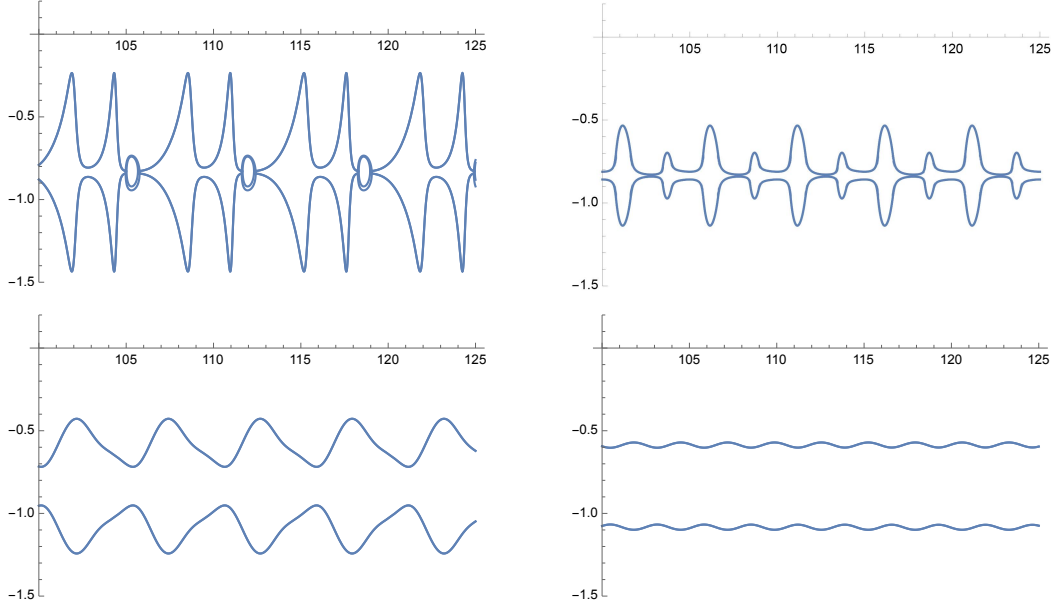


Figure 9: Real parts of eigenvalues for the four primary biped gaits (plotted against time) are negative for the parameter values used in simulations in [94, Section 14]. *Top left: hop. Top right: run. Bottom left: jump. Bottom right: walk.*

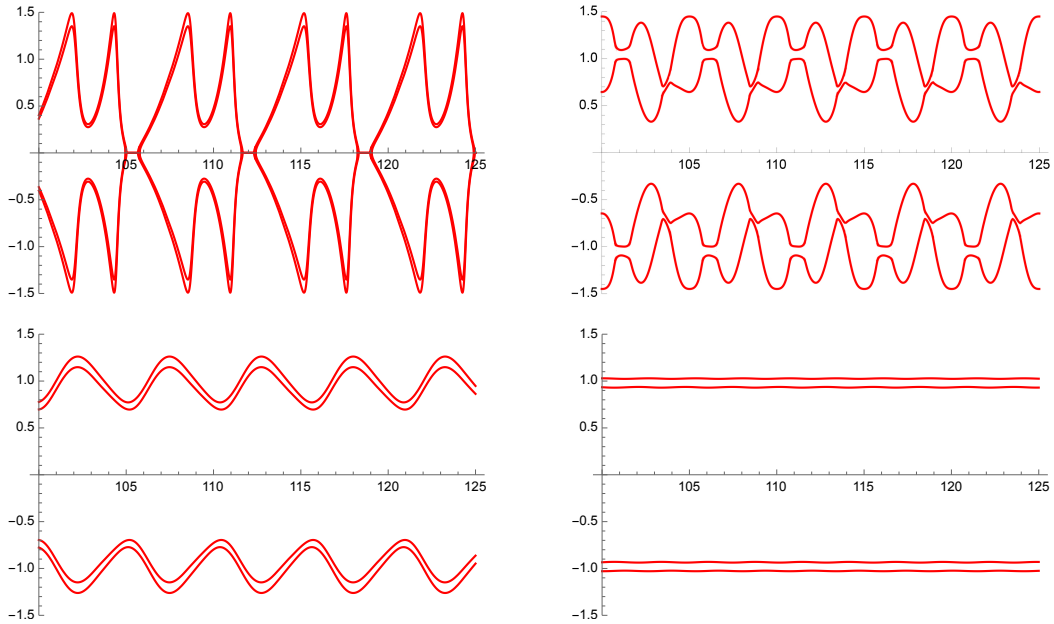


Figure 10: Imaginary parts of eigenvalues for the four primary biped gaits (plotted against time) are negative for the parameter values used in simulations in [94, Section 14]. *Top left: hop. Top right: run. Bottom left: jump. Bottom right: walk.*

$I = 1.1, g = 1.8$ . (Actually [94] uses  $I = 0.8$  for the hop, but we replace this here by 1.1.)

The other parameters are:

$$\begin{aligned}
\text{hop} &: \quad \alpha = 0.5 \quad \beta = 0.6 \quad \gamma = 0.8 \\
\text{run} &: \quad \alpha = -0.5 \quad \beta = -0.6 \quad \gamma = 0.8 \\
\text{jump} &: \quad \alpha = -0.5 \quad \beta = 0.6 \quad \gamma = -0.8 \\
\text{walk} &: \quad \alpha = 0.5 \quad \beta = -0.6 \quad \gamma = -0.8
\end{aligned}$$

The results for the 1-node module of Figure 3 (top) are listed below in Table 3, which also lists the period and the transverse Floquet multipliers.

The period and CPG Floquet multipliers for the 2-node module of Figure 3 (bottom) are the same as in Table 3. The transverse Floquet multipliers for the 2-node module are listed in Table 4.

## 4.5 Transverse Floquet Multipliers, 1-Node Module

We begin with Figure 3 (top), which is a genuine feedforward lift. It is enough to consider the transverse Floquet equation for node 5. Use the notation  $\alpha, \beta, \gamma$  of [94] for connection strengths, and let the CPG periodic orbit be

$$\begin{aligned}
&(x_1^E, x_2^E, x_3^E, x_4^E, x_1^H, x_2^H, x_3^H, x_4^H) = \\
&(a_1^E(t), a_2^E(t), a_3^E(t), a_4^E(t), a_1^H(t), a_2^H(t), a_3^H(t), a_4^H(t))
\end{aligned}$$

this is:

$$\begin{aligned}
\varepsilon \dot{x}_5^E &= -x_5^E + \mathcal{G}(-gx_5^H + \beta a_2^E(t) + \gamma a_3^E(t) + \alpha a_4^E(t) + I) \\
\dot{x}_5^H &= x_5^E - x_5^H
\end{aligned} \tag{4.17}$$

Here the inputs  $x_3^E(t), x_4^E(t), x_5^E(t)$  are evaluated on the periodic orbit of the CPG using (4.13), and the parameters  $\varepsilon, \alpha, \beta, \gamma, g, I$  refer to that equation.

Numerical computation shows that all four gaits are Floquet-stable at the parameter values stated above. The computed data (truncated to 3 significant figures, four for the period) are shown in Table 3.

The transverse Floquet multipliers are generally smaller by a few orders of magnitude than the CPG Floquet multipliers, indicating a high degree of stability of the lifted periodic orbit.

**Remark 4.1.** As regards the starred entries in Table 3, it is observed in [68] that in numerical integration of Floquet equations: ‘The accuracy of the computed trivial multiplier is not always comparable to the accuracy of the computed periodic solution and the accuracy of the other computed multipliers.’

## 4.6 Transverse Floquet Multipliers, 2-Node Module

For the 2-node module, with the same parameters for the CPG, the Floquet multipliers for the CPG are unchanged, so the periodic orbits are Floquet-stable. The transverse Floquet multipliers change, and we compute them to get table 4. Again, all gaits are Floquet-stable for these parameters, and the transverse Floquet multipliers are generally

gait	$T$	CPG multipliers	abs.	trans. multipliers	abs.
Hop stable	6.646	0.999*	0.999	0.00172	0.00172
		0.00117	0.00117	0.0000188	0.0000188
		0.000946	0.000946		
		0.000400	0.000400		
		0.000258	0.000258		
		0.0000143	0.0000143		
		$4.27 \times 10^{-6}$	$4.27 \times 10^{-6}$		
		$2.35 \times 10^{-6}$	$2.35 \times 10^{-6}$		
Run stable	4.991	1	1	0.00685	0.00685
		0.150	0.150	0.000571	0.000571
		0.00714	0.00714		
		0.00110	0.00110		
		0.000322	0.000322		
		0.000166	0.000166		
		0.0000773	0.0000773		
		0.0000497	0.0000497		
Jump stable	5.257	1	1	0.00522	0.00522
		0.505	0.505	0.000389	0.000389
		$0.000180 \pm 0.000387i$	0.000427		
		$0.000180 \pm 0.000111i$	0.000212		
		$0.0000580 \pm 0.0000273i$	0.0000641		
Walk stable	5.368	0.998*	0.998	0.00470	0.00470
		0.916	0.916	0.000325	0.000325
		$-8.09 \times 10^{-6} \pm 0.000424i$	0.000424		
		$0.0000531 \pm 0.0000914i$	0.000105		
		$0.0000452 \pm 0.0000322i$	0.0000555		

Table 3: CPG and transverse Floquet multipliers for the four gaits of the biped model with a 1-node module, Figure 3 (top). The CPG periodic orbit and the lifted periodic orbit are stable for all four parameter sets. All entries stated to three significant figures after the decimal point. \*These entries are presumably 1 with small numerical error. See Remark 4.1.

smaller by a few orders of magnitude than the CPG Floquet multipliers, indicating a high degree of stability of the lifted periodic orbit.

The main conclusion is that in this case, replacing feedforward arrows by lateral arrows does not affect the stability significantly.

## 4.7 Parameters for which Proposition 3.7 Applies

To facilitate comparison with [94] we have used the parameters values of that paper, where  $g = 1.8$  and the gain function is (4.14). However, this this value is slightly too big to apply Proposition 3.5, which requires  $g < 1.5$ . We now exhibit different simulations if the four primary gaits for  $g = 1.4$ , so that Proposition 3.7 applies.

gait	transverse multipliers	absolute value
Hop stable	0.0184	0.0184
	0.000322	0.000322
	0.000216	0.000216
	$3.16 \times 10^{-6}$	$3.16 \times 10^{-6}$
Run stable	0.0281	0.0281
	0.0190	0.0190
	0.000283	0.000283
	0.000102	0.000102
Jump stable	$0.000576 \pm 0.0182 i$	0.0182
	$0.0000931 \pm 0.0000614 i$	0.000111
Walk stable	$-0.00498 \pm 0.0199 i$	0.0205
	$0.0000502 \pm 0.0000559 i$	0.0000751

Table 4: Transverse Floquet multipliers for the four gaits of the biped model with a 2-node module, Figure 3 (bottom). The CPG periodic orbit and the lifted periodic orbit are stable for all four parameter sets. All entries stated to three significant figures after the decimal point.

We take the following parameter values for the four gaits:

$$\text{Hop: } I = 0.7 \quad \alpha = 0.5 \quad \beta = 0.6 \quad \gamma = 0.8 \quad g = 1.4 \quad \varepsilon = 0.5 \quad (4.18)$$

$$\text{Jump: } I = 1.1 \quad \alpha = -0.5 \quad \beta = 0.6 \quad \gamma = -0.8 \quad g = 1.4 \quad \varepsilon = 0.5 \quad (4.19)$$

$$\text{Run: } I = 1.1 \quad \alpha = -0.5 \quad \beta = -0.6 \quad \gamma = 0.8 \quad g = 1.4 \quad \varepsilon = 0.5 \quad (4.20)$$

$$\text{Walk: } I = 1.1 \quad \alpha = 0.5 \quad \beta = -0.6 \quad \gamma = -0.8 \quad g = 1.4 \quad \varepsilon = 0.5 \quad (4.21)$$

Proposition 3.5 does not apply with these parameters because  $\varepsilon = 0.5$  and this requires  $g < 2.22474/2 = 1.11237$ . However, Proposition 3.7 does apply, since when  $\varepsilon = 0.5$  this requires  $g < 4.82843/2 = 2.41411$ , so these gaits are transversely Liapunov Stable for the stated parameter values.

More refined estimates are also possible, because the range of values taken by  $\eta(t)$  in (3.5) need not include  $x = 1$ , where  $\mathcal{G}'(x)$  attains its maximum value of  $2s$ . In Figure 11 all oscillations are less than 1. The maxima are roughly

$$\begin{aligned} \text{hop} & : 0.97 \\ \text{jump} & : 0.46 \\ \text{run} & : 0.69 \\ \text{walk} & : 0.37 \end{aligned}$$

Since  $\mathcal{G}'(x)$  is monotone increasing for  $x < 1$  the corresponding bounds for  $g$  are 1.52, 28.95, 5.25, and 58.67. Thus the estimates needed for the jump, run, and walk are more generous. With other values of  $\varepsilon$ , modified estimates of this kind can prove transverse Floquet stability when Proposition 3.5 does not apply. We do not attempt to state such modified estimates in general, but there is clearly scope for further improvements.

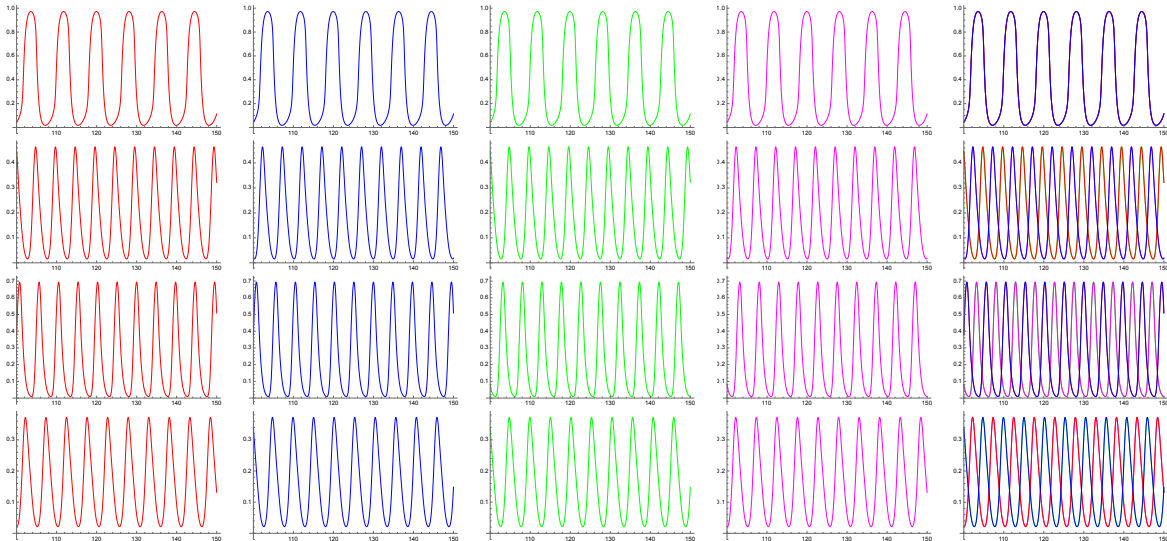


Figure 11: Time series of selected activity variables for a rate model of Figure 3 (top). Each row shows  $x_i^E$  for  $1 \leq i \leq 4$ , followed by all nodes in the chain (up to node 8) superposed. *From top to bottom*: hop, jump, run, walk.

## 5 Conclusions

Regular phase patterns are common in networks of dynamical systems with suitable symmetries, which in particular suggests modeling animal gait patterns using symmetric networks. Animal gaits are widely thought to be created by a central pattern generator (CPG), located in the spinal column. Several model CPGs have been studied previously from the viewpoint of symmetric dynamics.

Networks with feedforward lift structure (CPG + chain) naturally propagate synchronous or phase-synchronous states along linear chains. This type of network topology suggests new and physiologically plausible networks for animal locomotion, which we analysed in the case of bipeds. We studied two such feedforward lifts using a CPG proposed by Pinto and Golubitsky [87] and extending it along a chain of arbitrary length formed from ‘modules’ that are copies of the CPG.

An important issue is the stability of the propagating signals. This splits into stability under synchrony-preserving perturbations (stability for the CPG) and stability under synchrony-breaking perturbations (transverse stability). This decomposition was discussed in [99] for several stability notions, and was specialized here to the two feedforward lifts. Using a rate model, we established Floquet stability (for suitable parameters) using numerical calculations of CPG and transverse Floquet multipliers. Liapunov stability was established analytically using two Liapunov functions.

Feedforward lifts provide a simple, effective, and robust way to propagate signals with specific synchrony and phase patterns in a stable manner. They suggest biologically plausible topologies for neuronal networks that propagate such signals.

## References

- [1] S. Aoi, D. Katayama, S. Fujiki, T. Kohda, K. Senda, and K. Tsuchiya. Cusp catastrophe embedded in gait transition of a quadruped robot driven by nonlinear oscillators with phase resetting, *Proc. 2012 IEEE Internat. Conf. Robotics and Biomimetics*, Guangzhou (2012) 384–389.
- [2] S. Arber and R.M. Costa. Connecting neuronal circuits for movement, *Science* **360** (2018) 1403–1404.
- [3] Aristotle. De partibus animalium, de inessu animalium, de motu animalium, in: *Parts of Animals, Movement of Animals, Progression of Animals* (transl. A.S. Peek and E.S. Forster), Harvard University Press, Cambridge MA 1936.
- [4] P. Ashwin, J. Buescu, and I. Stewart. Bubbling of attractors and synchronization of chaotic oscillators, *Phys. Lett. A* **193** (1994) 126–139.
- [5] P. Ashwin, J. Buescu, and I. Stewart. From attractor to chaotic saddle: a tale of transverse instability, *Nonlinearity* **9** (1996) 703–737.
- [6] A. Berkowitz. Expanding our horizons: central pattern generation in the context of complex activity sequences, *J. Exp. Biol.* **222** (2019) 192054.
- [7] P. Boldi and S. Vigna. Fibrations of graphs, *Discrete Math.* **243** (2002) 21–66.
- [8] P.-L. Buono. Models of central pattern generators for quadruped locomotion: II. Secondary gaits, *J. Math. Biol.* **42** (2001) 327–346.
- [9] P.-L. Buono and M. Golubitsky. Models of central pattern generators for quadruped locomotion: I. Primary gaits, *J. Math. Biol.* **42** (2001) 291–326.
- [10] P.-L. Buono and A. Palacios. A mathematical model of motorneuron dynamics in the heartbeat of the leech, *Physica D* **188** (2004) 292–313.
- [11] R.L. Calabrese and E. Peterson. Neural control of heartbeat in the leech *Hirudo medicinalis*, in: *Neural Origin of Rhythmic Movements* (eds. A. Roberts and B. Roberts), *Symp. Soc. Exp. Biol.* **37** (1983) 195–221.
- [12] R.L. Calabrese, F. Nadim and Ø.H. Olsen. Heartbeat control in the medicinal leech: A model system for understanding the origin, coordination, and modulation of rhythmic motor patterns, *J. Neurobiol.* **27** (1995) 390–402.
- [13] J.D. Chambers, J.C. Bornstein, and E.A. Thomas. Insights into mechanisms of intestinal segmentation in guinea pigs: a combined computational modeling and in vitro study, *Am. J. Physiol. Gastrointest: Liver Physiol.* **295** (2008) G534–541.
- [14] J.D. Chambers, E.A. Thomas, and C. Bornstein. Mathematical modelling of enteric neural motor patterns, *Proc. Austral. Physiol. Soc.* (2013) **44** 75–84 .
- [15] J.J. Collins and S.A. Richmond. Hard-wired central pattern generators for quadrupedal locomotion, *Biol. Cybern.* **71** (1994) 375–385.
- [16] J.J. Collins and I. Stewart. Hexapodal gaits and coupled nonlinear oscillator models, *Biol. Cybern.* **68** (1993) 287–298.
- [17] J.J. Collins and I. Stewart. Coupled nonlinear oscillators and the symmetries of animal gaits, *J. Nonlin. Sci.* **3** (1993) 349–392.

- [18] A. Daigle. Not a betting man: Stanford, Muybridge, and the Palo Alto wager myth, *Film History* **29** (2017) 112–130.
- [19] C. Diekman, M. Golubitsky, T. McMillen, and Y. Wang. Reduction and dynamics of a generalized rivalry network with two learned patterns, *SIAM J. Appl. Dynam. Sys.* **11** (2012) 1270–1309.
- [20] M.B. Elowitz and S. Leibler. A synthetic oscillatory network of transcriptional regulators, *Nature* **403** (2000) 335–338.
- [21] G.B. Ermentrout and N. Kopell. Parabolic bursting in an excitable system coupled with a slow oscillation, *SIAM J. Appl. Math.* **46** (1986) 233–253.
- [22] B. Ermentrout and D. Terman. *The Mathematical Foundations of Neuroscience*, Springer, New York 2010.
- [23] R. FitzHugh. Impulses and physiological states in theoretical models of nerve membrane, *Biophys. J.* **1** (1961) 445–466.
- [24] G. Floquet. Sur les équations différentielles linéaires à coefficients périodiques, *Ann. École Norm. Sup. Paris* **12** (1883) 47–89.
- [25] J.B. Furness. *The Enteric Nervous System*, Blackwell, Oxford 2006.
- [26] P. Gambaryan. *How Mammals Run: Anatomical Adaptations*, Wiley, New York 1974.
- [27] W. Gerstner and W. Kistler. *Spiking Neuron Models*, Cambridge University Press, Cambridge 2002.
- [28] W. Gerstner, W. Kistler, R. Naud, and L. Paninski. *Neuronal Dynamics: from single neurons to networks and models of cognition*, Cambridge University Press, Cambridge 2014.
- [29] J. Gjorgjieva, J. Berni, J.F. Evers, and S.J. Egle. Neural circuits for peristaltic wave propagation in crawling *Drosophila* larvae: analysis and modeling, *Front. Comput. Neurosci.* **7** (2013); doi: 10.3389/fncom.2013.00024.
- [30] M. Golubitsky, D. Romano, and Y. Wang. Network periodic solutions: full oscillation and rigid synchrony, *Nonlinearity* **23** (2010) 3227–3243.
- [31] M. Golubitsky, D. Romano, and Y. Wang. Network periodic solutions: patterns of phase-shift synchrony, *Nonlinearity* **25** (2012) 1045–1074.
- [32] M. Golubitsky and I. Stewart. *The Symmetry Perspective, Progress in Mathematics* **200**, Birkhäuser, Basel 2002.
- [33] M. Golubitsky and I. Stewart. *Dynamics and Bifurcation in Networks*, SIAM, Philadelphia 2023.
- [34] M. Golubitsky, I. Stewart, P.-L. Buono, and J.J. Collins. A modular network for legged locomotion, *Physica D* **115** (1998) 56–72.
- [35] M. Golubitsky, I. Stewart, J.J. Collins, and P.-L. Buono. Symmetry in locomotor central pattern generators and animal gaits, *Nature* **401** (1999) 693–695.
- [36] M. Golubitsky, I. Stewart, and D.G. Schaeffer. *Singularities and Groups in Bifurcation Theory II*, Applied Mathematics Series, **69**, Springer, New York 1988.
- [37] M. Golubitsky, I. Stewart, and A. Török. Patterns of synchrony in coupled cell networks with multiple arrows, *SIAM J. Appl. Dynam. Sys.* **4** (2005) 78–100.

- [38] M. Gouolding. Circuits controlling vertebrate locomotion: moving in a new direction, *Nature Rev. Neurosci.* **10** (2009) 507–518.
- [39] J. Gray. *Animal Locomotion*, Weidenfeld and Nicolson, London 1968.
- [40] H. Gregersen. *Biomechanics of the Gastrointestinal Tract*, Springer, London 2003.
- [41] S. Grillner. The motor infrastructure: from ion channels to neuronal networks, *Nature Rev. Neurosci.* **4** (2003) 573–586.
- [42] S. Grillner and A. El Manira. Current principles of motor control, with special reference to vertebrate locomotion, *Physiol. Rev.* **100** (2020) 271–320.
- [43] S. Grillner and T.M. Jessell. Measured motion: searching for simplicity in spinal locomotor networks, *Curr. Opin. Neurobiol.* **19** (2009) 572–586.
- [44] J. Guckenheimer and P. Holmes. *Nonlinear Oscillations, Dynamical Systems, and Bifurcations of Vector Fields*, Springer, New York 1983.
- [45] S.E. Harris. *Horse Gaits, Balance and Movement*, Howell Book House, New York 1993.
- [46] B.D. Hassard, N.D. Kazarinoff, and Y.-H. Wan. *Theory and Applications of Hopf Bifurcation*, London Math. Soc. Lecture Notes **41**, Cambridge University Press, Cambridge 1981.
- [47] J.L. Hindmarsh and R.M. Rose. A model of neuronal bursting using three coupled first order differential equations, *Proc. Roy. Soc. Lond. B: Biological Sciences* **221** (1984) 87–102.
- [48] M.W. Hirsch and S. Smale. *Differential Equations, Dynamical Systems, and Linear Algebra*, Academic Press, New York 1974.
- [49] A.L. Hodgkin and A.F. Huxley. A quantitative description of membrane current and its application to conduction and excitation in nerve, *J. Physiol.* **117** (1952) 500–544.
- [50] V. In, A. Kho, P. Longhini, J.D. Neff, A. Palacios, and P.-L. Buono. Meet ANIBOT: the first biologically-inspired animal robot, *Internat. J. Bif. Chaos* **32** (2022); doi: 10.1142/S0218127422300014.
- [51] E.M. Izhikevich. *Dynamical Systems in Neuroscience: the geometry of excitability and bursting*, MIT Press, Cambridge MA 2010.
- [52] M. Jha and N.R. Chauhan. A review on snake-like continuum robots for medical surgeries, *IOP Conf. Ser.: Mater. Sci. Eng.* **691** (2019) 012093.
- [53] O. Kiehn. Locomotor circuits in the mammalian spinal cord, *Annu. Rev. Neurosci.* **29** (2006) 279–306.
- [54] N. Kopell. Towards a theory of modelling central pattern generators, in: *Neural Control of Rhythmic Movements in Vertebrates* (eds. A.H. Cohen, S. Rossignol, and S. Grillner), Wiley, New York 1988.
- [55] N. Kopell and G.B. Ermentrout. Symmetry and phaselocking in chains of weakly coupled oscillators, *Comm. Pure Appl. Math.* **39** (1986) 623–660.
- [56] N. Kopell and G.B. Ermentrout. Coupled oscillators and the design of central pattern generators, *Math. Biosci.* **89** (1988) 14–23.
- [57] N. Kopell and G.B. Ermentrout. Phase transitions and other phenomena in chains of oscillators, *SIAM J. Appl. Math.* **50** (1990) 1014–1052.

- [58] W.B. Kristan Jr., R.L. Calabrese, and W.O. Friesen. Neuronal control of leech behavior, *Progress in Neurobiol.* **76** (2005) 279–327.
- [59] W.A. Kunze and J.B. Furness. The enteric nervous system and regulation of intestinal motility, *Ann. Rev. Physiol.* **61** (1999) 117–42.
- [60] C.R. Laing and C.C. Chow. A spiking neuron model for binocular rivalry, *J. Comput. Neurosci.* **12** (2002) 39–53.
- [61] L. Lapique. Recherches quantitatives sur l’excitation électrique des nerfs traitée comme une polarisation, *Journal de Physiologie et de Pathologie Generale* **9** (1907) 620–635. Translated as: Quantitative investigations of electrical nerve excitation treated as polarization, *Biological Cybernetics* **97** (2007) 341–349.
- [62] J.P. LaSalle. Recent advances in Liapunov stability theory, *SIAM Rev.* **6** (1964) 1–11.
- [63] J.P. LaSalle and S. Lefschetz. *Stability by Lyapunov’s Second Method with Applications*, Academic Press, New York 1961.
- [64] I. Leifer, F. Morone, S.D.S. Reis, J.S. Andrade Jr., M. Sigman, and H.A. Makse. Circuits with broken fibration symmetries perform core logic computations in biological networks, *PLOS Computational Biology* (2020); doi: 10.1371/journal.pcbi.1007776 0.
- [65] A.M. Liapunov. *Obshchaya Zadacha Ustoichivosti Drizheniya*, Kharkov 1892, and *Comm. Soc. Math. Kharkov* **3** (1893) 265–272; French translation: Problème générale de la stabilité du mouvement, *Ann. Fac. Sci. Toulouse* **9** (1907) 203–474; reproduced as *Annals of Mathematics Studies* **17**, Princeton University Press, Princeton 1947; English translation: *Stability of Motion*, Academic Press, New York 1966.
- [66] H. Lindén, P.C. Petersen, M. Vestergaard, and R.W. Berg. Movement is governed by rotational neural dynamics in spinal motor networks, *Nature* **610** (2022) 526–531.
- [67] K.A. Lindsay, J.M. Ogden, D.M. Halliday, and J.R. Rosenberg. An introduction to the principles of neuronal modelling. In: U. Windhorst and H. Johansson (eds), *Modern Techniques in Neuroscience Research*, Springer, Berlin, Heidelberg 1999.
- [68] T. Luzyanina and K. Engelborghs. Computing Floquet multipliers for functional differential equations, *Internat. J. Bif. Chaos* **12** (2002) 2977–2989.
- [69] R.B. McGhee. Some finite state aspects of legged locomotion, *Math. Biosci.* **2** (1968) 67–84.
- [70] H.A. Makse, P. Boldi, F. Sorrentino, and I. Stewart. *Symmetries of Living Systems*, Cambridge University Press, Cambridge, to appear 2025.
- [71] R.A. Mann. Biomechanics, in: *Disorders of the Foot* (ed. M.H. Jahss), W.B. Saunders and Co., Philadelphia 1982 37–67.
- [72] R.A. Mann, G.T. Moran, and S.E. Dougherty. Comparative electromyography of the lower extremity in jogging, running and sprinting, *Amer. J. Sports Med.* **14** (1986) 501–510.
- [73] L. Markus and H. Yamabe. Global stability criteria for differential systems, *Osaka J. Math.* **12** (1960) 305–317.
- [74] D.A. McCrea and I. Rybak. Organization of mammalian locomotor rhythm and pattern generation, *Brain Res. Rev.* **57** (2008) 134–146.
- [75] J. Milnor. On the concept of attractor, *Commun. Math. Phys.* **99** (1985) 177–195.

- [76] C. Morris and H. Lecar. Voltage oscillations in the barnacle giant muscle fiber, *Biophys. J.* **35** (1981)193–213.
- [77] Z. Mu, H. Wang, W. Xu, T. Liu, and H. Wang. Two types of snake-like robots for complex environment exploration: Design, development, and experiment, *Adv. Mech. Eng.* **9** (2017); doi: 10.1177/1687814017721.
- [78] R.M. Murray, Z. Li, and S.S. Sastry. *A Mathematical Introduction to Robotic Manipulation*, CRC Press, Boca Raton 1993.
- [79] E. Muybridge. *Animals in Motion*, Chapman and Hall, London 1899; reprinted Dover, New York 1957.
- [80] J. Nagumo, S. Arimoto, and S. Yoshizawa. An active pulse transmission line simulating nerve axon, *Proc IRE* **50** (1962) 2061–2070.
- [81] A. Nair, D.S. Kadam, R. Menon, and P.C. Shende. Neural differential equations: a comprehensive review and applications, *Advances in Nonlinear Variational Inequalities* **28** (2025) 146–160.
- [82] E. Olivares, E.J. Izquierdo, and R.D. Beer. A neuromechanical model of multiple network rhythmic pattern generators for forward locomotion in *C. elegans*, *Front. Comput. Neurosci.* **18** (2021); doi: 10.3380/fncom.2021.572339.
- [83] M. Parker and I. Stewart. A new mechanism for intermittency in rings of cells, *Internat. J. Bif. Chaos* **18** (2008) 675–687.
- [84] L.M. Pecora. Synchronisation of oscillators in complex networks, *Pramana J. Phys.* **70** (2008) 1175–1198.
- [85] L.M. Pecora and M. Barahona. Synchronisation of oscillators in complex networks, *Chaos Complex. Lett.* **1** (2005) 61–91.
- [86] L.M. Pecora and T.L. Carroll. Master stability functions for synchronized coupled systems. *Phys. Rev. Lett.* **80** (1998) 2109–2112
- [87] C.A. Pinto and M. Golubitsky. Central pattern generators for bipedal locomotion, *J. Math. Biol.* **53** (2006) 474–489.
- [88] O. Purcell, N.J. Savery, C.S. Grierson, and M. di Bernardo. A comparative analysis of synthetic genetic oscillators, *J. R. Soc. Interface* (2010) **7** 1503–1524; doi:10.1098/rsif.2010.0183.
- [89] J. Rinzel and B. Ermentrout. Analysis of neural excitability and oscillations, in: *Methods in Neuronal Modeling* (I. Segev I and C. Koch, eds.), MIT Press, Cambridge MA 1998, 251–291.
- [90] K. Sakamoto, Z. Soh, M. Suzuki, Y. Iino, and T. Tsuji. Forward and backward locomotion patterns in *C. elegans* generated by a connectome-based model simulation, *Nature Scientific Reports* **11** (2021) 13737; doi: 10.1038/s41598-021-92690-2.
- [91] G. Schöner, W.Y. Jiang, and J.A.S. Kelso. A synergetic theory of quadrupedal gaits and gait transitions, *J. Theor. Biol.* **142** (1990) 359–391.
- [92] S. Seok, C. D. Onal, R. Wood, D. Rus, and S. Kim. Peristaltic locomotion with antagonistic actuators in soft robotics, *2010 IEEE International Conference on Robotics and Automation* (2010) 1228–1233; doi: 10.1109/ROBOT.2010.5509542.
- [93] A. Shpiro, R. Curtu, J. Rinzel and N. Rubin. Dynamical characteristics common to neuronal competition models, *J. Neurophysiol.* **97** (2007) 462–473.

- [94] I. Stewart. Symmetry-breaking in a rate model for a biped locomotion central pattern generator, *Symmetry* **6** (2014) 23–66.
- [95] I. Stewart. Overdetermined ODEs and rigid periodic states in network dynamics, *Portugaliae Mathematica* **79** (2022) 85–161.
- [96] I. Stewart, M. Golubitsky, and M. Pivato. Symmetry groupoids and patterns of synchrony in coupled cell networks, *SIAM J. Appl. Dyn. Sys.* **2** (2003) 609–646.
- [97] I. Stewart and M. Parker. Periodic dynamics of coupled cell networks II: cyclic symmetry, *Dynamical Systems* **23** (2008) 17–41.
- [98] I. Stewart, S.D.S Reis, and H.A. Makse. Dynamics and bifurcations in genetic circuits with fibration symmetries, *J. R. Soc. Interface* **21** (2024) 20240386.
- [99] I. Stewart and D. Wood. Stable synchronous propagation of signals by feedforward networks, *SIAM J. Appl. Dyn. Sys.* **23** (2024), doi: 10.1137/23M1552267.
- [100] I. Stewart and D. Wood. Synchronous propagation of signals by feedforward networks of standard model neurons, *Internat. J. Bif. Chaos* (30th anniversary issue), to appear 2025.
- [101] A.E. Talpalar, J. Bouvier, L Borgius, G Fortin, A Pierani, and O. Kiehn. Dual-mode operation of neuronal networks involved in left-right alternation, *Nature* **500** (2013) 85–88.
- [102] W.J. Thompson and G.S. Stent. Neuronal control of heartbeat in the medicinal leech II: Inter-segmental coordination of heart motor neuron activity by heart interneurons, *J. Comput. Physiol.* **111** (1976) 281–307.
- [103] A. Wenning, A.A. Hill, and R.L. Calabrese. Heartbeat control in leeches. I: Fictive motor pattern, *J. Neurophysiol.* **91** (2004) 397–409.
- [104] Wikipedia. Biological neuron model, [en.wikipedia.org/wiki/Biological\\_neuron\\_model](https://en.wikipedia.org/wiki/Biological_neuron_model), 2 February 2025.
- [105] H.R. Wilson and J.D. Cowan. Excitatory and inhibitory interactions in localized populations of model neurons, *Biophys. J.* **12** (1972) 1–24.
- [106] Y. Zhong, L. Hu, and Y. Xu. Recent advances in design and actuation of continuum robots for medical applications, *Actuators* **9** (2020) 142; doi: 10.3390/act9040142.